THESIS FOR THE DEGREE OF DOCTOR OF PHILOSOPHY

Tar and Condensable Hydrocarbons in Indirect Gasification Systems

Mikael Israelsson

Department of Energy and Environment

CHALMERS UNIVERSITY OF TECHNOLOGY

Gothenburg, Sweden 2016

Tar and Condensable Hydrocarbons in Indirect Gasification Systems
Mikael Israelsson
ISBN: 978-91-7597-395-1

Doktorsavhandling vid Chalmers tekniska högskola
Ny serie Nr. 4076
ISSN 0346-718X

Department of Energy and Environment
Division of Energy Technology
Chalmers University of Technology
SE-412 96 Gothenburg
Sweden
Telephone + 46 (0)31-772 1000

Printed in Sweden
Chalmers Reproservice
Gothenburg 2016

Tar and Condensable Hydrocarbons in Indirect Gasification Systems

Mikael Israelsson
Division of Energy Technology
Chalmers University of Technology
SE-412 96 Gothenburg (Sweden)

Abstract

Biomass gasification, which is a primary process step in the production of biofuels, yields a combustible gas mixture (raw gas). This raw gas consists of a wide range of species, from permanent gases to condensable hydrocarbons, which are collectively known as tar. Considered as the Achilles heel of biomass gasification, tar starts to condense at temperatures of around 350°C, causing blockage and fouling of downstream equipment. In addition to creating operational difficulties, tar is responsible for a loss of efficiency if it is not successfully converted into permanent gases. Consequently, there is a need to understand the concepts underlying tar formation and evolution, so as to guide efforts towards reducing its yield, as well as towards facilitating its removal once formed. This requires accurate quantification of all the components of the produced raw gas to evaluate the behavior of the tar. However, as the produced gas comprise such a wide range of species, several different measurement techniques are required. In this work, the effects of catalytic materials on tar were investigated in two different systems. The observed responses motivated the development of improved measurement systems, directed to fulfilling the mass balance of the gasifier. These systems were subsequently implemented to map the behaviors of the various species of the raw gas, for a range of process parameters, and to derive a reaction scheme for all the condensable species.

The concepts of primary and secondary measures were studied by introducing a catalytic material directly into the Chalmers dual fluidized bed (DFB) gasifier (primary measure) and by utilizing an additional reactor for catalytic reforming of the raw gas (secondary measure). Overall, both measures resulted in significantly decreased levels of tar. However, the composition of the remaining tar differed for the two measures, as did the added amounts of oxygen.

The SPA method for tar measurement was evaluated for reproducibility, which was found to be well within 10% for the majority of the measured species. In addition, the detection limits of the SPA method have been extended throughout this work and currently extend from benzene to coronene. A high-temperature reactor, for thermal cracking of all the gas species into CO, CO_2, H_2, and H_2O, was constructed to measure the total elemental yields of C, H, O, and N in the raw gas. This measurement allowed a mass balance for the system to be constructed, which combined with the cold gas and tar measurements, was used to obtain information regarding the yields and composition of previously unmeasured condensable species. This group contained a level of carbon similar to that found in the SPA-measured tar, thereby underlining the need for quantification through standard measurements.

The developed measurement equipment was used to map the behavior of the gasifier under various temperatures, residence times, and steam-to-fuel ratios. The performed measurements showed that not only are the previously unmeasured species important for fulfilling the mass balance of the gasifier, but also for describing the formation of SPA-measureable tar. Subsequent modeling of the tar formation and evolution for the measured cases revealed that a substantial fraction of these species tends to form tertiary SPA tar directly, as these species are reformed. Furthermore, it was shown that additional factors, presumably related to the aging of the bed material, can significantly affect the reactivity of the gasifier and should be quantified to improve the functionality of the model.

Keywords: Tar, condensable species, SPA, CLR, DFB, CS, UCS, HTR.

List of Publications Included in the Thesis

I. Fredrik Lind, Mikael Israelsson, Martin Seemann, Henrik Thunman. Manganese oxide as catalyst for tar cleaning of biomass-derived gas. *Journal of Biomass and Biorefinery*, 2012, 2, (2), pp 133-140.

II. Anton Larsson, Mikael Israelsson, Fredrik Lind, Martin Seemann, Henrik Thunman. Using ilmenite to reduce the tar yield in a dual fluidized bed gasification system. *Energy & Fuels*, 2014, 28, pp 632−2644.

III. Mikael Israelsson, Martin Seemann, Henrik Thunman. Assessment of the solid-phase adsorption method for sampling biomass-derived tar in industrial environments. *Energy & Fuels*, 2013, 27, pp 7569−7578.

IV. Mikael Israelsson, Anton Larsson, Henrik Thunman. Online measurement of elemental yields, oxygen transport, condensable compounds, and heating values in gasification systems. *Energy & Fuels*, 2014, 28 (9), pp 5892-5901.

V. Mikael Israelsson, Teresa Berdugo Vilches, Henrik Thunman. Conversion of condensable hydrocarbons in a dual fluidized bed biomass gasifier. *Energy & Fuels*, 2015, 29, pp 6465-6475.

VI. Mikael Israelsson, Henrik Thunman. Gasification reaction pathways of condensable hydrocarbons. *Accepted for publication. Energy & Fuels.*

Mikael Israelsson is the principal author of Papers III, IV, V and VI. Fredrik Lind and Anton Larsson are the principal authors of Papers I and II, respectively, Mikael Israelsson contributed with tar analysis, evaluation, and editing to Papers I and II. Assistant Professor Martin Seemann, who is the assistant academic supervisor, participated in the experimental work and contributed ideas and editorial support. Professor Henrik Thunman, who is the principal academic supervisor, contributed ideas, discussions and editorial comments to all the papers.

Publications not Included in the Thesis

- Nicolas Berguerand, Fredrik Lind, Mikael Israelsson, Martin Seemann, Serge Biollaz, Henrik Thunman. Use of nickel oxide as a catalyst for tar elimination in a chemical–looping reforming reactor operated with biomass producer gas. *Ind. Eng. Chem. Res*., 2012, 51 (51), pp 16610-16616.

- Henrik Leion, Erik Jerndal, Britt-Marie Steenari, Simon Hermansson, Mikael Israelsson, Erik Jansson, Martin Johnsson, Rebecka Thunberg, Albin Vadenbo, Tobias Mattisson, Anders Lyngfelt. Solid fuels in chemical-looping combustion using oxide scale and unprocessed iron ore as oxygen carriers. *Fuel*, 2009, 88, pp 1945-1954.

Acknowledgments

First I would like to thank my main supervisor professor Henrik Thunman for giving me the opportunity to pursue a PhD and for always taking the time to support me in all aspects of my work. I also thank my assistant supervisor, associate professor Martin Seemann for all his help and discussions concerning measurements and experiments.

A special thanks to Fredrik Lind who, while not technically required to, can always be relied upon to help a colleague in need, and Anton Larsson for being a good friend and sounding board.

Large scale experiments is a team effort and I have been lucky to be working alongside some truly fantastic people. Anton Larsson, Jelena Marinkovic, and Teresa Berdugo Vilches, thank you for all your help, it has been great to work with you. Research engineers Jessica Bohwalli, Rustan Hvitt, Johannes Öhlin, and Ulf Stenman, thank you for helping us all so much. To Nicolas, Huong, Alberto, Erik, and the rest of the gasification group, thanks for everything. I also wish to thank the operating staff at Akademiska Hus for making sure everything is working perfectly.

Thank you everyone at the division of energy technology for creating a fantastic work environment, especially Olivia for being so patient when I'm trying to speak Spanish.

Finally, I would like to thank my family, friends, and my darling Carin for all their support.

This work has been financially supported by E.ON AB, Akademiska Hus, Göteborg Energi AB, Valmet AB (previously Metso Power AB), the Swedish Energy Agency, and Chalmers Energy Initiative. The latter part of this work was performed within the Competency Center of the Svenskt Förgasningscentrum (SFC).

Mikael Israelsson, Göteborg 2016

Table of Contents

1 - Introduction

The production of biofuels from local or regional biomass resources represents a secure supply of fuel with reduction of CO_2 emissions, with the added benefit of creating and retaining jobs within the forest industry. This study focuses on biomass gasification, which is a primary process step towards the production of biofuels, in which the fuel undergoes thermochemical conversion to yield a combustible gas. Currently, several process types are available for the gasification of biomass, encompassing a range of operational temperatures, pressures, fuel types, and means of generating the heat necessary for conversion [1, 2].

The present study focuses on measurements that are coupled to indirect dual fluidized bed (DFB) gasification, wherein part of the fuel is combusted in a circulating fluidized bed (CFB) so as to generate heat for the gasification of the remaining fuel (Figure 1). The generated heat is transported from the combustor to the gasifier by means of a bed material which, in combustion processes, is usually composed of silica sand. However, in DFB gasification, natural ores, such as olivine, ilmenite, bauxite or any other economically feasible material, are often used[3-5]. In Figure 1, biomass is introduced to the gasifier, which is operated as a bubbling fluidized bed (BFB) and is fluidized using steam. The biomass is subsequently dried, devolatilized, and partially gasified due to the high temperature, yielding a combustible gas mixture called raw gas. The unconverted char enters the combustor together with the bed material, where it is combusted to generate heat for the gasifier. The alternative to indirect gasification is direct gasification wherein all steps of the fuel conversion takes place in one reactor by only adding enough combustion air to maintain the required temperature. The main advantage of indirect, as opposed to direct gasification, is that the gas produced contains lower levels of CO_2 and N_2, due to the fact that the combustion occurs separately while the gasifier is fluidized using only steam. Conversely, the advantages of direct gasification are its abilities to operate at higher temperatures and pressures, as only one process vessel is utilized for the fuel conversion. However, it is noteworthy that the heating value of the gas produced by indirect gasification is generally higher (due to it being less diluted) than that produced by indirect gasification.

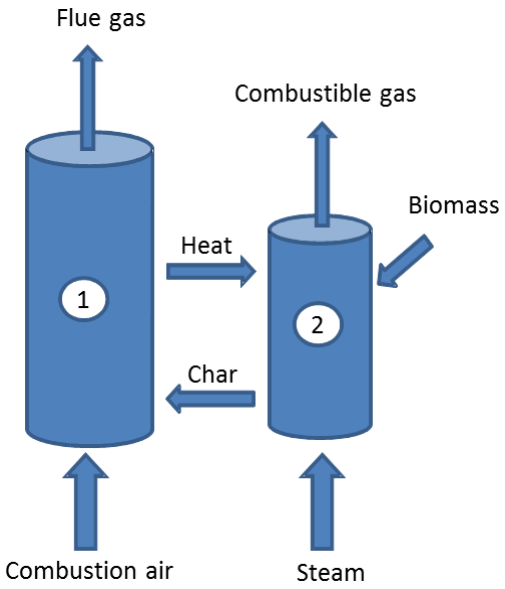

Figure 1: Schematic of a DFB gasifier, which consists of: 1, a CFB combustor; and 2, a BFB gasifier.

With the possible exception of gasification at extremely high temperatures, all available gasification techniques produce a raw gas that contains a broad spectrum of species. This spectrum of gases encompasses species that range in size from hydrogen and methane to heavy, condensable organic species, which are commonly referred to as 'tar'[2]. Tar is an unwanted byproduct that poses an enduring challenge to gasification, as described by Tom Reed (1998, adopted from Milne[2]):

> *"While a great deal of time and money has been spent on biomass gasification in the last two decades, there are very few truly commercial gasifiers, operating without government support or subsidies, day in, day out, generating useful gas from biomass. The typical project starts with new ideas, announcements at meetings, construction of the new gasifier. Then it is found that the gas contains 0.1-10% 'tars.' The rest of the time and money is spent trying to solve this problem. Most of the gasifier projects then quietly disappear. In some cases the cost of cleaning up the experimental site exceeds the cost of the project! Thus 'tars' can be considered the Achilles heel of biomass gasification. In the gasification of coal, a more mature technology, the 'tars' (benzene, toluene, xylene, coal tar) are useful fuels and chemicals. The oxygenated 'tars' from biomass have only minor use. With current environmental and health concerns, we can no longer afford to relegate 'tars' to the nearest dump or stream."*

Tar is a rather loosely defined term in the literature. In this work, tar is defined as all organic species that have a boiling point above or equal to that of benzene (80°C). Furthermore, the raw gas is subdivided into the permanent gas or cold gas (comprising H_2, CO, CO_2, CH_4, C_2H_2, C_2H_4, C_2H_6, C_3H_6, He, N_2, and H_2S), steam, and condensable species (CS), which contain all the carbon-containing species in the raw gas (including tar) that are not found in the cold gas.

In line with the statement of Reed, any process in which the raw gas is further treated for biofuel production is significantly hindered if the raw gas has not been cleaned of tar prior to

the treatment. If the tar is not removed effectively the remaining tar may condense on the pipes and coolers and may deactivate catalysts in the downstream process, resulting in severe operational difficulties. Therefore, a comprehensive understanding of tar creation and maturation is needed to implement measures to control its formation and to facilitate its eventual removal. The different methods available for gas cleaning include: 1) separating the tar from the gas stream, such as scrubbing[6]; and 2) reforming the tar into light gas components[7, 8]. The benefit of the second method is that the energy content of the tar is retained in the gas.

1.1 Primary & Secondary Measures: Gas Cleaning

Scrubbing of the raw gas will, most likely, always be necessary to some extent due to the presence of steam and trace amounts of tar. However, there remains an incentive to pursue reforming methods, as they both increase the overall efficiency of the process and decrease the demand on the scrubber. Consequently, the complexity, and cost, of the reforming method employed is determined by the potential gains in terms of process efficiency and gas cleaning.

The methods for reforming the raw gas can be categorized into primary and secondary measures; two different methods are investigated in Papers 1 and 2. Primary measures are implemented within the gasifier, whereas secondary measures require the use of auxiliary equipment. In general, primary measures are cheaper in terms of cost and effort, so they are often implemented as the initial step towards reducing the tar content to an acceptable level. However, if the primary measure proves unsuccessful, secondary methods can be considered, provided that the potential gain outweighs the cost incurred.

Paper 2 describes the implementation of ilmenite ore as part of the bed material in the Chalmers 2–4-MW DFB gasifier. This active material is circulated together with the sand and transports heat to the gasifier, where it catalytically supports the conversion of tar and condensable species into lighter gases. The activity of the material decreases as it resides in the gasifier due to deactivation by sulfur and carbon deposits on the active surfaces. When the bed material enters the boiler, it is regenerated and heated as the deposits and char are combusted before the material re-enters the gasifier. An important feature of many active bed materials is their ability to transport oxygen from oxidizing to reducing environments *via* metallic species, such as iron. This phenomenon is fundamental for certain technologies, such as chemical-looping combustion (CLC)[9] and oxygen carrier-aided combustion (OCAC)[10]. This feature should be suppressed in gasification processes because the transported oxygen combusts the product gas, thereby reducing the efficiency. However, the required bed material flow is governed by the heat demand of the gasifier, which promotes a given level of oxygen transport for a given bed material.

Secondary measures for raw gas cleaning can be implemented through the use of secondary equipment or as an integrated part of the gasifier, e.g., the recirculation of fines to the freeboard[11]. For the secondary measure investigated in Paper 1, the produced raw gas was introduced into a secondary process vessel that contained the active material. Several different

approaches are possible for secondary tar cleaning, including single fluidized beds and packed beds containing a wide range of active materials[7]. Furthermore, secondary measures that do not utilize catalytic materials, e.g., thermal cracking, can be used. In this work, the secondary vessel is a chemical-looping reformer (CLR)[8], which is a dual fluidized bed that contains manganese ore. The dual beds operate in a way that is similar to the combustor and gasifier. The catalyst transports heat and oxygen to the reformer, where it reforms tar and condensable species, after which it is regenerated and heated in the air reactor. The required circulation rate of the bed material is determined by the deactivation and the heat transport that is needed to sustain the endothermic reactions of the reformer. However, since the heat required for gasification is supplied within the gasifier, the circulation rate in the CLR can be lower, resulting in a lower level of oxygen transport.

The main benefits of secondary equipment measures for tar reduction include the ability to control, to some extent, the oxygen transport and the possibility to separate the active material from the ash in the fuel (which can cause agglomeration). Furthermore, it is likely that higher levels of tar conversion can be attained, since the process can be optimized without taking into consideration the gasifier operation. However, the need for auxiliary equipment increases significantly the complexity and cost of the overall process. A clear understanding of process performance is needed to decide which type of measure is required to achieve a satisfactory level of tar reduction. Consequently, the ability to measure and/or predict the tar yield in the raw gas is important for the design of the gas cleaning equipment.

1.2 Quantification of Fuel Conversion

The establishment of a satisfactory mass balance requires reliable measurements of a majority of the in- and out-going streams of a gasifier. This requirement places serious demands on measurements performed in DFB units, as the flow of unconverted fuel from the combustor is difficult to measure directly. However, similar difficulties are experienced with direct gasification, as unconverted fuel either accumulates or exits with the gas and ash removal streams. Consequently, the raw gas stream needs to be quantified in terms of the total elemental flows, cold gas, CS, and steam content to describe accurately the fuel conversion, efficiency, tar yield, and other parameters of interest. Figure 2 depicts the steam-free raw gas in terms of the cold gas, condensable species (CS), tar (as measured using the SPA method, described in Paper 3), unidentified condensable species (UCS), and the total elemental yields of C, H, O, and N. While other elements, such as S and Cl, could also be included in the total elemental yields, the present study focuses on streams that are sufficiently large to be of relevance to the overall mass balance.

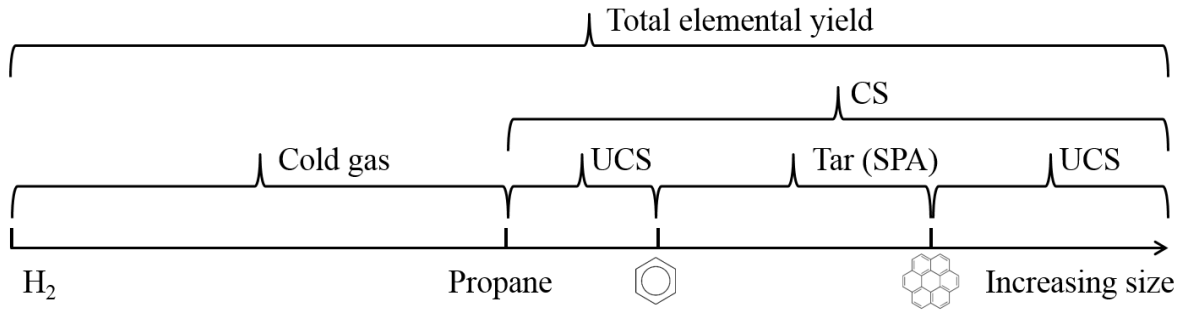

Figure 2: Components of the raw gas spectrum.

The permanent gases, which are often collectively referred to as the cold gas, are cleaned of tar and steam using a gas conditioning system, after which the dried gas is quantified using a micro-gas chromatograph (micro-GC). Thus, the number of species detectable in the cold gas is restricted by the analysis equipment, as well as the gas conditioning system. In this work, the cold gas contains species that range from hydrogen to propane. Furthermore, the total flows of the cold gas components are quantified by adding a known flow of helium to the steam used to fluidize the gasifier. Due to the difficulties with online steam measurements related to the presence of particles and condensing tar species, the steam content of the raw gas is often estimated through condensation, using the gas conditioning system. However, this estimation is time-consuming and difficult to perform accurately because stable operation is required.

There are currently several methods that enable offline and online measurements of tar[12-18]. Most of the online methods are more suitable for monitoring trends in the tar levels, as they do not differentiate between the different tar species. The two main offline methods, the European tar protocol[17] and solid phase adsorption (SPA)[18-20], are better suited to assessing mass balances because they allow the identification of individual species. These two methods differ mainly in terms of the mode of sampling. The European tar protocol is a cold trapping method, whereby tar is condensed in a series of impinger bottles filled with a solvent. In contrast, in the SPA method, a small amount of raw gas is extracted through a column that contains an amine which adsorbs the tar. The tar is subsequently removed from the column through eluation, using a solvent. For both these methods, the dissolved tar is analyzed by GC-FID or GC-MS.

In this study, the SPA method was chosen for tar analysis on the grounds that it requires less time and less sophisticated equipment for sample collection. Furthermore, the ability to collect several samples simultaneously allows evaluation of reproducibility. The accuracy, reproducibility, and measurable species of the SPA method were investigated in Paper 3, to assess its suitability for monitoring tar behavior in large-scale systems.

The gas conditioning system for analysis of the cold gas, used together with the SPA method for tar analysis, enables the quantification and identification of most of the carbon-containing species in the raw gas. Unfortunately, as both measurements are restricted with respect to which species they can measure, the UCS in the raw gas (Fig. 2) are not measured. The UCS

include species that are not readily measured using a GC, e.g., GC-undetectable and gravimetric tar[17], as well as soot and light gas species that lie (in terms of boiling point) between propane and benzene.

To resolve the issues related to incomplete quantification, Neves *et al.*[21] have proposed a method for the quantification of C, H, O, and N in the raw gas that involves combusting the gas prior to the analysis. This method enables determinations of the total elemental flows in the raw gas using simple equipment, such as a NDIR system or micro-GC. The developed system was used successfully to measure the raw gas from the Chalmers 2–4-MW DFB gasifier. Furthermore, the results of the performed experiments raised the possibility of obtaining even higher levels of accuracy using this type of measurement. Paper 4 investigates the possibility of improving the method proposed by Neves *et al.*[21] by thermal cracking of the raw gas. Heating the raw gas to 1700°C induces rapid decomposition of complex species into CO, CO_2, H_2O, and H_2, with very low yields of soot. The main benefit of thermal cracking, as compared to combustion, is that all the uncertainties linked to the reactant gas (in terms of flow and composition) are avoided. Furthermore, the reformed gas is not diluted by the nitrogen present in the combustion air. The fact that nitrogen is not added also allows the nitrogen measurement to be used to detect leaks. The resulting gas mixture was analyzed in a micro-GC to obtain the total elemental flows of C, H, O, and N in the raw gas. This allowed indirect determination of the amount of UCS, as the elemental flows of the raw gas were compared with the elemental flows of the cold gas and SPA-detectable tar.

Use of the high-temperature reactor (HTR) to quantify completely the raw gas allows the mass balance of the gasifier to be fulfilled. As a result, additional parameters, such as the total fuel conversion, char conversion, and oxygen transport in DFB systems, can be determined. Furthermore, the energy balance of the system can be refined to estimate the energy content of the condensable species, in addition to the heating value of the raw gas. This provides valuable information as to which actions can be motivated in terms of primary and secondary measures for tar cleaning. The ability to perform this type of measurement also simplifies the process of describing the effects of alternating process conditions, as much of the speculation surrounding unmeasured components becomes unnecessary.

1.3 Gasification Process Parameters

The use of active materials in the gasifier is an effective primary measure for reducing the levels of tar and altering the composition of the cold gas. However, varying the process parameters, such as the temperature and gas residence time inside the gasifier, exemplifies primary measures that can strongly influence the raw gas composition. Unlike the optional use of active materials, the effects of these parameters will always be present in gasification, which highlights the importance of understanding their influences on the energy and mass balances of the gasification process.

Paper 5 investigates the effects of altering the average raw gas temperature, the level of fluidization (steam-to-fuel ratio), and the raw gas residence time within the gasifier, using the

measuring equipment developed in Papers 3 and 4. The raw gas temperature is controlled by the temperature of the ingoing bed material, which in turn is governed by the boiler temperature. Changing the temperature of the raw gas also induces a slight change in the residence time of the raw gas. The level of fluidization in the gasifier is varied to generate experimental points for different steam-to-fuel ratios, resulting in different concentrations of steam in the raw gas. Increasing the level of fluidization also shortens the gas residence time and causes additional bed material to be thrown up into the freeboard of the gasifier. As a consequence, there is increased gas-solid contact and a slightly higher raw gas temperature due to the increase in heat transfer between the bed and raw gas. The average gas residence time in the gasifier is varied by simultaneously changing the fuel feed and the level of fluidization, thereby maintaining a constant steam-to-fuel ratio. This has the same effects on the gas-solid contact as when only the level of fluidization is changed. In summary, varying any one process parameter inevitably affects other parameters that influence gasifier performance.

1.4 Evolution of Condensable Species

Several studies have presented reaction schemes for tar, describing its formation from the primary species generated during pyrolysis[22-24], as well as through the reformation of already mature tar[25-27]. Unfortunately, many of these studies have been based on incomplete mass balances or have relied on species that are not measured, making validation difficult. A global reaction mechanism that includes the formation, subsequent maturation, and decomposition of tar, preferably based entirely on measureable species, would bring together all the previously mentioned reaction schemes.

The results obtained in Paper 5 describe clearly how all the relevant aspects of the carbon mass balance are affected by the employed process parameters. This raises the possibility of constructing a reaction scheme for the condensable species in which all the segments are represented as measured components, i.e., not just the tar and cold gas. Thus, the aim of Paper 6 was to construct an expanded (yet simplified) reaction scheme based on the measurements presented in Paper 5.

1.5 Aim and Outline

The aim of this thesis was to identify and develop the tools necessary to describe the evolution of tar, while taking into account the effects of other condensable and cold gas species. The ability to measure and predict the behavior of tar enables the design of improved processes for its minimization and removal. The thesis encompasses the concept of tar formation, evolution, and conversion in indirect biomass gasification systems.

The outline of the work conducted in this thesis is presented in Figure 3. The structure of the thesis itself reflects that of the outline to show clearly the levels of measurements associated with the different experiments. Papers 1 and 2 investigate the use of catalytic materials to reduce the tar levels in the produced raw gas. However, these papers also show the importance of comprehensive and accurate measurements to allow any conclusions to be

drawn from the experiments. Paper 3 presents an assessment of the SPA method for tar quantification with the aim of determining its detection limits and accuracy. The work included in Paper 3 was conducted alongside that of Papers 1 and 2 and motivated the efforts to fulfill the mass balance of the gasifier in Paper 4. The HTR used in Paper 4 was designed to quantify the total elemental flows of the raw gas. The performance of the HTR was experimentally validated and subsequently evaluated using the Chalmers DFB gasifier. The measurements presented in Papers 5 and 6 were performed using an improved version of the SPA method and with minor changes being made to the HTR. Paper 5 investigates the effects of process parameters, such as temperature and residence time, on the raw gas composition and tar evolution. In Paper 6, the data obtained in Paper 5 are further examined to develop the reaction scheme required to explain the trends in CS and tar formation and evolution. In addition, key parameters and conversion routes for the construction of a comprehensive model for CS are identified.

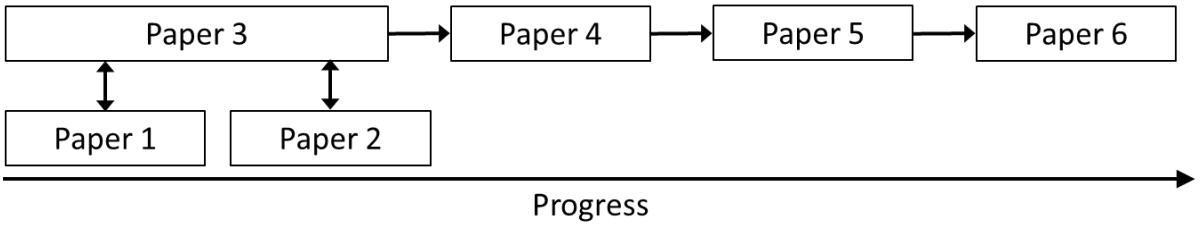

Figure 3: Outline of the thesis.

2 - Theory

2.1 Tar Mechanisms

Tar is formed during the fuel pyrolysis and subsequently matures according to Figure 4 depending on the surrounding conditions. Overall, as the temperature is increased, the composition shifts from a relatively high oxygen to carbon ratio to zero and the tar becomes more aromatic and stable in nature.

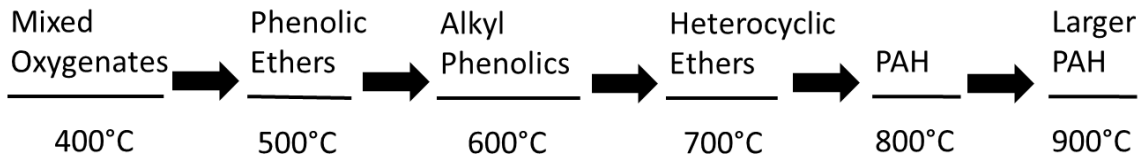

Figure 4: Tar maturation scheme proposed by Elliott (1988), as adopted from Milne et al.[2].

The scheme depicted in Figure 4 offers valuable insights into the effects of temperature on tar maturation. However, for the construction of a useful model of tar evolution, a more sophisticated scheme is needed. Numerous studies have modeled the reactivity of tar[23, 25, 28, 29], based on experiments that utilized single tar species[30-32] and synthetic mixtures, as well as various types of biomass[33, 34]. The derived reaction schemes differ in terms of their complexity, ranging from those that describe the evolution of predominant species as a function of temperature[2] to those that establish reaction schemes that contain several tar species, whereby stable species are formed from the decomposition of less stable species[23, 24, 27]. Furthermore, the schemes differ with regard to the processes that they describe. For example, certain studies[25-27] describe the evolution of an already mature tar spectrum that contains stable species, such as benzene, while that of Font Palma[23] employs a scheme in which primary tar is formed from lignin and progressively matures into secondary and tertiary tar.

Earlier studies of pyrolysis and gasification have shown that the tar spectrum consists of several hundred different species during the evolution from primary to mature tar[33]. Since not all of these species can be included in a model, they are categorized into groups and each group is represented by a model compound. The chosen model compound is usually the most abundant species in a specific group. As an example, phenol is often used to represent either phenolic species or all tar species that contain oxygen. The chosen model components or groups differ across different studies[23, 25, 26]. For example, Corella *et al.*[25] constructed a

model based on benzene, 1-ring compounds, naphthalene, 2-ring compounds, 3- and 4-ring compounds, and phenolic compounds. Depending on the reactions included in the model, the choice of groups may limit the tar evolution, thereby restricting the tar to decomposition into gas or rearrangement into other species. As a result, the contributions of light gas species, UCS, soot, and GC-undetectable tar[35] to the total tar levels are disregarded. Unsaturated, light hydrocarbons can form or add to the structure of already existing aromatic species *via* the Diels-Alder reaction (R1), followed by dehydrogenation[22, 36, 37], the HACA mechanism (R2)[28, 37, 38] or the combination of species, such as cyclopentadiene (R3)[22, 23, 26, 39]. Furthermore, the decay of UCS, GC-undetectable or gravimetric tar may yield measureable tar species.

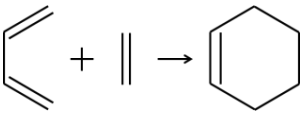

(R1)

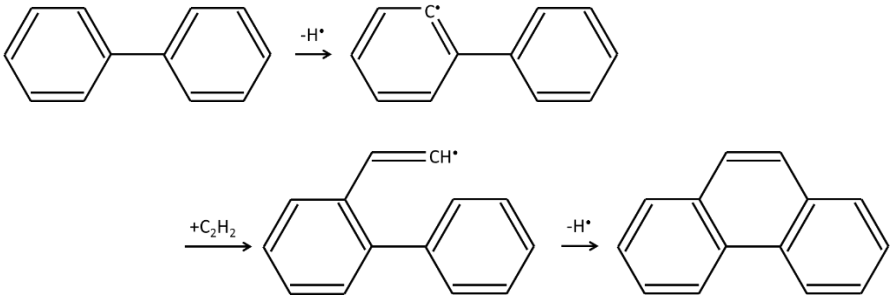

(R2)

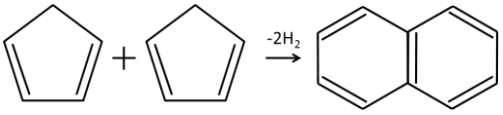

(R3)

GC-undetectable and gravimetric tar species are generally referred to as being very heavy, which implies that they are comprised of several aromatic rings in a soot-like structure, resulting in low H/C-ratios (<0.5). Fuentes-Cano *et al*.[37] performed measurements wherein they determined the elemental composition of the gravimetric tar fraction for temperatures in the range of 600°–900°C, giving corresponding H/C-ratios in the range of approximately 1.5–1.2. The determined ratios are significantly higher than those expected from soot-like species and are similar to the H/C-ratio of the employed fuel (1.7). This suggests that the collected sample consists of unconverted fuel fragments or primary tar components (Fig. 4). Regardless of the precise nature of the gravimetric tar, it is plausible that its decomposition would generate both GC-detectable tar and gas species.

As soot consists primarily of carbon, steam gasification of soot is assumed to yield only CO and H_2. While this assumption is probably valid for many applications, pyrolysis experiments performed on soot derived from pine combustion[38] resulted in a weight loss of 27% at

400°C, consisting of aromatic tar species. In conclusion, if significant levels of gravimetric tar, light hydrocarbons and soot are generated, the effects of these groups on the measureable tar should be considered. A reoccurring trend in the literature that supports the possibility of hidden source terms for tar is the optimum temperature for maximum tar yield[28, 35, 40]. Scott *et al*.[40] found maximum tar yields at 500°–550°C for pyrolysis; this was also noted by Morf *et al*.[28] but was disregarded as an outlier as it was not reproducible. A similar trend, albeit at a higher temperature range (750°–800°C), was described by Kiel *et al*.[35]. While this initial increase in tar level may not be relevant for processes that operate at higher temperatures, it implies that measureable tar can be generated outside of the primary pyrolysis. Consequently, the quantification of all segments of the raw gas spectrum is a perquisite for describing accurately the behavior of tar.

2.2 Primary and Secondary Measures

The introduction of catalytic materials directly to the gasifier as a primary measure or *via* secondary equipment, with the aim of reducing the tar yield, has been studied extensively[2, 7, 41, 42]. In addition to reducing the tar yield, catalytic materials often increase hydrogen production *via* the WGSR, resulting in increased levels of CO_2. For DFB systems, metal-containing catalytic materials generate a certain degree of oxygen transport, as the particles are oxidized in the combustor and are subsequently reduced in the gasifier[9]. Some of the transported oxygen is likely to react with various tar species, resulting in a decreased yield of tar. Nevertheless, the majority of the transported oxygen will react with cold gas species, decreasing gasifier efficiency. A previous study[41] has shown that the catalytic potency of ilmenite increases as it is reduced, which implies that oxygen transport not only decreases process efficiency, but it also reduces the effective use of the catalyst.

The two approaches to catalytic gas cleaning reported in Papers 1 and 2 differ mainly with respect to the choice of catalyst and the level of oxygen transport. An additional and potentially important difference is the level of maturity of the gas as it comes into contact with the catalyst. The gas that enters the CLR has already experienced the time/temperature history of the gasifier and is, most likely, significantly different from the newly formed gas that comes into contact with the active bed material of the gasifier. Unfortunately, the tar yield of the CLR relative to the fuel feed could not be obtained, as the mass balance of the CLR was not satisfied. Consequently, the two measurements are compared on the basis of as-measured concentrations and the composition of the measured tar. In line with Paper 1, the tar spectrum was divided into seven groups, based on size and composition, as follows: phenols; benzene; 1-ring aromatic species with branches; naphthalene; 2-ring aromatic species with branches; 3- and 4-ring aromatic species; and unknown components. The selected groups correspond to those used by Corella *et al*.[25], with the exception that unknown tar species constitute a distinct group. This grouping system was chosen because it separates the different species on the basis of size and reactivity. Typically, the branched species and phenols are more easily converted than are the pure aromatic components. In addition, while the identities of the unknown tar species are (by definition) unknown, their behaviors generally reflect

those of the branched species. Therefore, they were placed in their own group, so as to clarify the analysis of the other groups.

Previous work conducted by Larsson *et al.*[43] describes how the performance of a gasifier and its auxiliary systems can be estimated by considering only the inter-relationships between the syngas species CO, CO_2, and H_2. The expected changes in the H/C and O/C molar ratios of the syngas species due to the WGSR, char gasification, methane reforming, and oxygen transport (combustion) are depicted as separate lines in Figure 5. The point of origin corresponds to pyrolysis at 800°C[44], and as the WGSR proceeds, all the CO present at this point is eventually converted into CO_2 and H_2. Similarly, as oxygen is added to the gas mixture, H_2 and CO are combusted to an equal extent, yielding a syngas that consists of CO_2. In contrast, reactions that add carbon to the syngas may decrease the O/C ratio, and may even increase the H/C ratio of the pyrolysis gas. Some reactions, such as methane-reforming reactions, greatly affect the syngas composition and, intuitively, similar lines for the conversion of other hydrocarbons would fall between those of char gasification and methane reforming. In summary, the variations in the concentrations of the syngas species can yield valuable information concerning the observed gasification process.

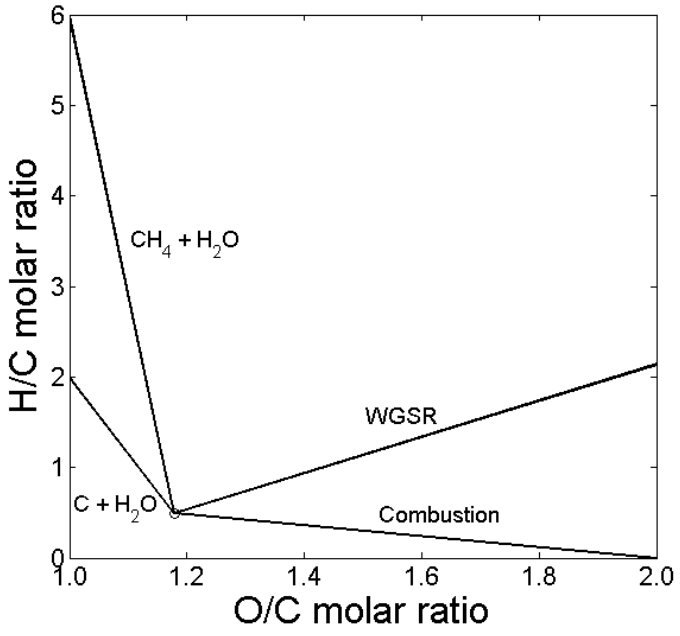

Figure 5: Changes in the H/C and O/C molar ratios of the syngas produced during pyrolysis due to the WGSR, char gasification, methane reforming, and oxygen transport (combustion)[43].

2.3 Measurement Techniques

The different measurements and streams associated with the gasifier are shown in Figure 6. The inward flows of fuel, steam, and trace gas (helium) are continuously monitored and controlled[45]. The helium is added to the steam prior to it entering the gasifier, to ensure even distribution throughout the gasifier. The rotary valve, which introduces fuel to the gasifier, is purged using dried flue gas from the boiler. The amount of flue gas that enters the gasifier is calculated based on the level of nitrogen in the cold gas. The bed material flow is determined by the operation of the boiler and is responsible for the transport of heat, unconverted fuel, and oxygen between the boiler and gasifier. The CLR, high-temperature reactor (HTR), and gas-conditioning system, for the separation of condensable species (CS), operate on a slipstream of raw gas.

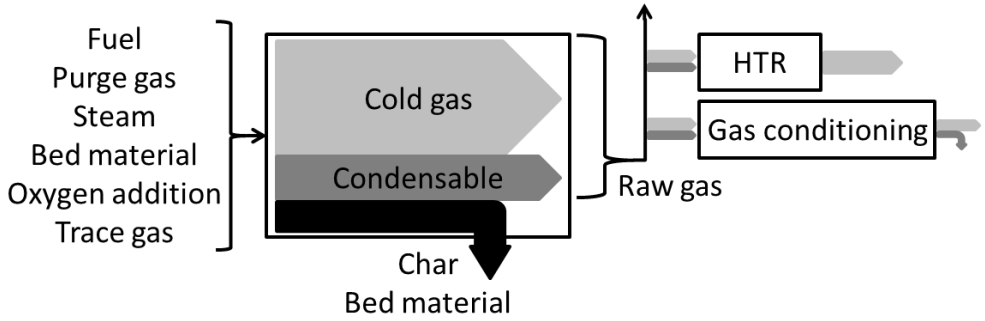

Figure 6: Overview of the flows in the gasifier. HTR, high-temperature reactor.

2.3.1 Tar Analysis

The importance of appropriate sample acquisition is discussed in Paper 3, together with additional factors that may affect the sampled gas. Regardless of the measurement technique employed, the required slipstream extraction point, transport tubes, and potential dust filters should interfere as little as possible with the gas composition.

As previously stated, the main difference between the SPA method and the European tar protocol is the procedure used for sample collection. A previous study by Osipovs[19] compared the two methods, which yielded similar results for species heavier than xylene. Osipovs used a secondary adsorbent column to improve the measurement of the lighter species benzene, toluene, and xylene (BTX); however, the core amount of heavier species was adsorbed in the first column. The sampling time for one SPA sample is roughly 1 min, which means that several samples can be collected in rapid succession, allowing the detection of fluctuations in gasifier performance. The comparatively long sampling times involved in the tar protocol (typically 30−60 min)[18] render it impractical for the determination of rapid fluctuations, which are instead represented as a mean value. If the process variations are large, the above can complicate the matching of the tar data to the measured gas data, as gas measurements are typically carried out at a significantly higher frequency. The long sampling times of the tar protocol also make it difficult to compare different sample results from the same experimental point, so as to determine the error of measurement. A faster version of

cold trapping developed at the Paul Scherrer Institute in Switzerland (PSI)[46] can be used for resolving variations in the tar output. However, this method still requires the use of a solvent on-site, as well as similar amounts of equipment.

The SPA method described by Brage *et al.*[18] utilizes a 500-mg LC-NH_2 column for tar adsorption. However, as shown in Paper 3, the reproducibility obtained for BTX species is not comparable to that for heavier species, such as naphthalene. This has been reported previously[47] and has been confirmed through measurements performed in the Chalmers DFB gasifier using a 500-mg LC-NH_2 column that also contained active carbon (unpublished data). As a result, all the presented values for benzene and toluene reported in Papers 1–4 are to be considered as indicative at best. The carbon-containing columns were used for the experiments reported in Papers 5–6, resulting in reliable measurements of all species within the range from benzene to coronene.

2.3.2 High-Temperature Reactor

The HTR induces the decomposition of larger molecules into primarily CO, CO_2, H_2, and H_2O, which are more readily measurable than the entire raw gas spectrum. The thermal decomposition of various tar components in argon has been thoroughly investigated[30, 31], revealing significant conversion at temperatures in the range of 700°–1000°C and residence times of 5 seconds. Similar measurements, in which soot formation was also determined, were performed using steam with shorter residence times at higher temperatures[32]. Jess[32] achieved complete conversion of naphthalene at 1300°–1400°C, with maximum yields of other tar components and soot at 1100°C and 1250°C, respectively. At 1400°C, the amount of soot decreased, although it was still significant. These findings imply that the temperature and residence times needed for satisfactory conversion to light gases are not dictated by the conversion of tar, but rather by the subsequent gasification of soot. Near-complete conversion of the soot is crucial for this method, as all the carbon that remains as soot will cause an error in the mass balance, resulting in seemingly lower yields of carbon and condensable species.

The HTR system allows on-line measurements of elemental yields through comparisons of the molar flow rates of the fuel feed and the gas leaving the HTR, according to:

$$\frac{\dot{n}_{i,HTR\ dry\ gas}}{\dot{n}_{i,fuel}}\left(1 \pm E_{tot,i}\right) = \frac{\dot{n}_{i,HTR\ dry\ gas}\left(1\pm E_{meas.,i}\right)}{\dot{n}_{i,fuel}\left(1\pm E_{fuel,i}\right)} = \frac{\sum_j \dot{n}_{j,HTR\ dry\ gas} Y_{i,j}\left(1\pm \varepsilon_{meas.,j}\right)}{\dot{n}_{i,fuel}\left(1\pm E_{fuel,i}\right)} \quad (1)$$

where $\dot{n}$ is a molar flow [mol/s], ε describes the degree of error of a specific measurement, and E describes the lumped error of a specific process stream or element. The different elements (C, H, O and N) are represented by i, while j denotes the various gas components, which include CO, CO_2, H_2, and CH_4. $Y_{i,\,j}$ is the molar content of element i in gas component j [mol/mol]. The measurement error ($\varepsilon_{meas.,j}$) is mainly dependent upon the uncertainty concerning the composition of the calibration gases, which is determined to within 1% relative to the given concentration for all the species. Similar to all measurements in which a measured parameter is related to the fuel feed, uncertainties related to the fuel composition can significantly affect the calculated yields of C, O, and H. Consequently, the fuel feed,

moisture content, and composition, as well as the composition of the char, need to be determined during the measurements.

As previously stated, helium was premixed with the steam feed of the gasifier and used as a trace gas to determine the molar flows of the dried gas according to:

$$\dot{n}_{j,dry\ gas} = \frac{C_{j,dry\ gas}}{C_{He,dry\ gas}} * \dot{n}_{He} \qquad (2)$$

where C is a measured molar concentration [mol/m^3]. The implementation of Eqs. (1) and (2), together with the fuel flow and composition, allows determinations of the carbon-based fuel conversion to raw gas, the char conversion, and the oxygen addition in CFB systems, as described in Paper 4.

Operating the HTR system in parallel with a gas-conditioning system permits the acquisition of useful additional information. When the two systems are synchronized, the measurements can be compared, so as to yield indirect measurements of the amount and average composition of the CS, which comprise all the raw gas species that are not found in the cold gas. In combination with known process parameters, such as the fuel and steam feeds, the two systems can be operated (as shown in Figure 7) to monitor the C, H, O, and N molar balances in the gasifier.

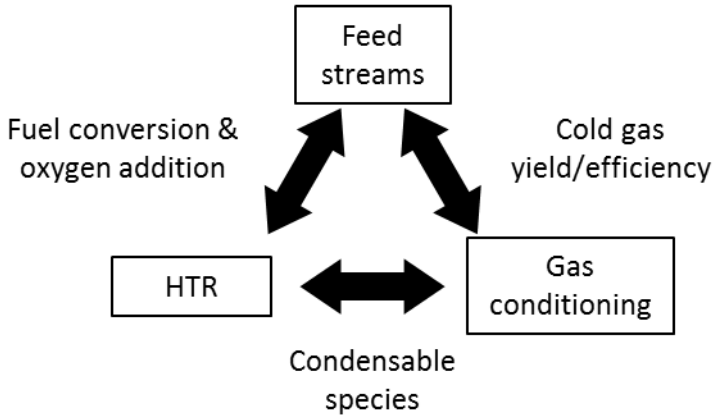

Figure 7: Flow of the data that are included in the mass balance.

Comparison of the data from the gas-conditioning system, G, and the data from the HTR can be done on two levels: with and without SPA analysis of the tar. If the tar measurement is omitted, the comparison is rapid and yields information as to the amount and average C, O, H composition of all the CS that are not measured by the gas conditioning system, as follows:

$$\dot{n}_{i,CS} = \dot{n}_{i,HTR}(1 \pm \varepsilon_{i,HTR,meas.}) + \dot{n}_{i,HTR,H_2O} - \dot{n}_{i,G}(1 \pm \varepsilon_{i,G,meas.}) - \dot{n}_{i,G,H_2O} \qquad (3)$$

where H_2O represents the condensed steam after the HTR and gas-conditioning system. Errors in the measured amounts of condensate after both systems will affect the determined oxygen and hydrogen contents of the CS. The errors related to the characterization of the CS are also

dependent upon the gas measurement. However, as two separate gas measurements are used, i.e., one for the gas-conditioning system and one for the HTR gas, the impact of the analysis error depends on the differences between the two systems in terms of the measured concentrations of a specified component. For instance, if there are low levels of tar and other decomposable components in the raw gas, the difference in the volumetric helium concentration between the two systems will be minor. Similar values for the measured helium concentrations will entail almost identical systematic errors of analysis, provided that the two systems were calibrated using the same gas. Consequently, the resulting total error for helium will be small. Conversely, for large differences in the concentrations of helium, the resulting error will approach that of the calibration gases.

In Paper 4, the accuracy and detection limit of the measurement of the CS are estimated by varying the concentrations of all the species randomly, assuming normally distributed probabilities, based on the given accuracies of the calibration gases. The main purpose of the HTR system is to quantify product streams that are relevant for the overall mass and heat balances. Therefore, while a low detection limit is desirable, other methods will be more suitable for the quantification and identification of low levels of CS[17, 18].

If the tar is measured using the SPA method, the UCS can be quantified in a manner similar to that employed in Eq. (3) by subtracting the yield of measured tar from the yield of CS. As previously mentioned, the UCS can contain several different types of species that are not measured as cold gas or SPA tar, such as semi-volatile gases, GC-undetectable/gravimetric tar, and even highly oxygenated species[48]. For the work presented in Paper 4, this group also contains some species (ranging from benzene to xylene) that are not completely quantified using the 500 mg of aminopropyl-bonded silica adsorbent in the SPA columns[47]. Regardless of the nature of this group, its quantification allows a deeper understanding of the gas-phase chemistry in gasification.

2.3.3 Average Composition of Condensable Species

Both methods used for the determination of the CS, i.e., with or without SPA analysis, require fast and accurate measurements of the steam in the raw gas, to determine with accuracy the oxygen and hydrogen fractions of the indirectly measured components. If the steam is not measured, the condensate terms in Eq. (3) can be omitted. As a result, the average oxygen and hydrogen contents of the CS will include an unknown fraction of H_2O:

$$C_iH_jO_k = C_iH_{j-2x}O_{k-x} + xH_2O \quad (4)$$

The lowest possible H/C ratio of the CS can be determined by setting x=k, thereby removing all the oxygen as water. The minimum H/C ratio, hereinafter referred to as CH_{min}, contains information on the average size of the CS or UCS, as well as their average heating value:

$$CH_{min} = \frac{j-2*k}{i} \quad (5)$$

A CH_{min} value in the range of 2–4 implies that the CS mixture mainly consists of alkanes, while CH_{min} values in the range of 0.5–1.0 suggest the presence of aromatic species. However, species with high O/C ratios, such as acrylic acid ($C_3H_4O_2$) and furan (C_4H_4O), have CH_{min} values of 0 and 0.5, respectively. Thus, low CH_{min} values may result from large PAHs or small oxygenated species.

The CH_{min} value varies between measurements, as a function of varying levels of conversion, which complicates the determination of a representative molecule. Consequently, in Paper 6, the UCS are described as a mixture of two pseudo-species, namely butane C_4H_{10} (B) and formic acid CH_2O_2 (F), thereby permitting the existence of a wide range of CH_{min} values for the UCS. As the individual CH_{min} values of B and F are 2.5 and -2.0, respectively, this approach reflects not only changes in the total carbon content of the UCS, but also changes in C, O, and H composition.

2.3.4 Average Energy Content of Condensable Species

The lower heating values (LHV), on a mass basis, vary significantly for different hydrocarbon species, making it challenging to estimate the energy content of the CS. As an alternative approach, the amount of released energy per reacted O_2 molecule needed for combustion [kJ/mole O_2] can be determined for compound A ($C_iH_jO_k$) as follows:

$$LHV_{O_2,A} = \frac{\Delta_f H^0_{g,A} - i * \Delta_f H^0_{g,CO_2} - {}^{j}/_{2} * \Delta_f H^0_{g,H_2O}}{i + {}^{j}/_{4} - {}^{k}/_{2}} \quad (6)$$

Implementation of the oxygen-based LHV makes it possible to determine the energy content of the CS using only the amount of carbon and the CH_{min} value. Furthermore, whether or not the "true" component A contains oxygen is irrelevant, i.e., $x \neq k$ in Eq. (4), as this will not affect the amount of oxygen required for combustion. The calculated LHV and CH_{min} values of compounds derived from pyrolysis[33] and gasification, as well as those of various alkanes, alkenes, and alcohols are presented in Table 1. Overall, the mean value of the oxygen-based LHV for all three groups is 422.9 kJ/mole O_2, with a standard deviation of 11.7 kJ/mole O_2, or 2.8% if one assumes equal amounts of all the species. The accuracy of this approach for determining a heating value is debatable, although it offers a fairly narrow range within which the correct value can be expected. As the CS most probably represent a mixture of compounds, large deviations from the determined mean value are unlikely. Furthermore, the energy contained in the CS accounts for roughly 10% of the energy in the fuel[45]. Thus, errors as large as 10% in the oxygen-based LHV will only induce an error of the order of ≤1% in the overall energy balance.

Table 1: Calculated CH_{min} and oxygen-based LHV values for species present during pyrolysis and gasification.

Method	CH_{min} Range (mean)	LHV [kJ/mole O_2] Range (mean)	Included species
Pyrolysis excluding SPA	0–2.0 (0.79)	418.7–460.3 (436.9)	ethene, acetaldehyde, acetic acid, acetone, acrylic acid, furan, 2-butanone, cyclopentanone, furfural, furfuryl alcohol
SPA tar	0.5–1.25 (0.78)	414.5–431.9 (421.9)	benzene, phenol, toluene, o-cresol, styrene, benzofuran, m/p-xylene, indene, naphthalene, 1-naphthol, 2-methylnaphthalene, dibenzofuran, biphenyl, acenaphthylene, acenaphthene, xanthene, fluorene, phenanthrene, anthracene, fluoranthene, pyrene, triphenylene, coronene
Miscellaneous	0.5–3.0 (2.07)	408.1–438.4 (417.0)	ethane, ethanol, propane, propene, propanol, butane, butadiene, butanol, 1,4-butanediol, diacetyl, pentane, 1-pentene, pentanol, n-hexane, cyclohexane, 1-hexanol, heptane, octane, nonane, decane

The calculated average energy content of the CS can be combined with that of the dried cold gas to determine the raw gas efficiency according to:

$$\eta_{Raw\ gas} = \frac{\sum \dot{n}_{j,G} * LHV_{j,G} + \left(\dot{n}_{C,CS} + {}^{\dot{n}_{H_{min},CS}}/_{4}\right) * LHV_{O_2,CS}}{\dot{m}_{fuel} * LHV_{fuel}} \quad (7)$$

Similarly, the theoretical raw gas efficiency can be determined by calculating the energy in the converted fraction of the fuel, as follows:

$$\eta_{Raw\ gas,theor.} = \frac{\dot{m}_{fuel} * LHV_{fuel} - \dot{m}_{char} * LHV_{char}}{\dot{m}_{fuel} * LHV_{fuel}} \quad (8)$$

The resulting efficiency describes the maximum amount of energy in the raw gas that can be recovered from the energy in the fuel. The difference between the above efficiencies can be considered as the enthalpy change within the gasifier due to various reactions, including heat from the bed material that is chemically bound within the raw gas.

The combined energy contents of the dried cold gas and the CS can be used together with the total flow of raw gas to determine the LHV [in MJ/Nm^3] of the wet raw gas according to:

$$LHV_{Raw\ gas} = \frac{\sum \dot{n}_{j,G} * LHV_{j,G} + \left(\dot{n}_{C,CS} + {}^{\dot{n}_{H_{min},CS}}/_{4}\right) * LHV_{O_2,CS}}{\dot{V}_{Raw\ gas}} \quad (9)$$

where $\dot{V}$ is the total volumetric flow of the raw gas [in Nm^3/s], consisting of the cold gas flow, as measured by the gas-conditioning system, the steam flow, determined using the mass balance, and the flow of CS, which are assumed to be free of oxygen. Furthermore, in Paper 4, it is assumed that the average tar molecule contains six carbon atoms. However, this assumption is not so important, as the contribution to the total flow is minor.

The LHV of the raw gas, determined using Eq. (9), requires input data (Fig. 7). However, if a gas-conditioning system is not available, the data obtained using only the HTR can be used to determine equivalent LHVs. As an example, the methane-equivalent raw gas LHV is determined by rearranging the composition of the gas that exits the HTR into CH_4, H_2O, and CO_2. Although the choice of equivalent species is dependent upon the process type, the equivalent LHV nevertheless presents a simple means for process monitoring and control.

2.4 Influence of Gasifier Operating Conditions

The performance of a DFB gasifier is dictated by several factors, ranging from the reactor design and the employed bed material to operational parameters, such as temperature. The individual effects of these factors need to be determined to enable optimization of gasifier operation. Unfortunately, these determinations are challenging because many of the parameters influence other parameters. In Paper 5, measurements were performed to investigate the effects of temperature, the steam-to-fuel ratio, and the gas residence time (changing the level of fluidization at a constant steam-to-fuel ratio). As previously mentioned, changes in the level of fluidization also affect the extent of gas-particle contact. Nevertheless, since the gas-particle contact should be similar for the measurements in which the steam-to-fuel ratio and the residence time are varied, this factor can be somewhat isolated.

The operating temperature during gasification and pyrolysis is known to affect significantly the levels of the cold gas and tar species[28, 35, 37, 39, 40, 42, 48-50]. In general, higher gasification temperatures are linked to reduced tar yields, increased cold gas yields, and an increased WGSR. For example, Kiel *et al.*[35] reported increased levels for most of the cold gas species as the gasification temperature was increased. Unfortunately, in that study, only the measured concentrations were reported; if one assumes that the nitrogen yield is relatively constant, the yields of the other cold gas species should be increasing. Consequently, increasing the gasification temperature seems to enhance the total yield of cold gas due to increased conversion of char and/or CS. In the same study[35], the levels of tar (excluding benzene) initially increased as the temperature was raised, and this was followed by a decrease in the total concentration of tar and increases in the levels of heavier class 4 and 5 tar species. In contrast, if the measured values for benzene are included as tar, the total concentration increases continuously with temperature, implying that the yield of tar also increases. This is relevant, as it indicates the presence of additional species that clearly influence the yield of tar. These species, which are often referred to as “class 1 tar” in line

with the ECN classification[35], are considered to be heavy, GC-undetectable, compounds. However, as shown in Figure 2, these species are included in the UCS and could very well be smaller, oxygenated species.

The steam-to-fuel ratio or the steam-to-biomass ratio has been extensively studied[35, 37, 42, 45, 50-52] through the introduction of supplemental steam or the pre-wetting of the fuel. In general, increasing the amount of steam enhances the WGSR, resulting in higher yields of hydrogen and carbon dioxide. Higher steam-to-fuel ratios are typically linked to decreased tar levels, although the opposite has been observed for catalytic bed materials and/or higher pressures[51]. Furthermore, as previously stated, determining the effects of the steam-to-fuel ratio is complicated by the concomitant changes in gas-solid contact and residence time.

The effects of increasing the gas residence time can be investigated by either introducing varying amounts of fuel and gasifying agent to the gasifier or sampling the gas at different heights of the gasifier freeboard. The observed effects of increased residence times on tar concentration range from reduced levels of tar to constant levels of tar with altered composition[35, 42, 49]. According to Kiel *et al.*[35], the concentration of tar decreases as the residence time is increased, whereas if benzene is included as tar the total concentration of tar remains relatively constant. Reactions that can significantly affect the tar composition presumably generate some lighter gas species, thereby reducing the tar yield. Therefore, it is likely that the conversion of undetected species contributes to the levels of measureable tar components.

2.5 Reaction Scheme of the Condensable Species

A mature tar spectrum derived from primary tar components has been modeled in previous publications[23, 24]. In these models, the yield of primary tar is calculated based on either the lignin fraction of the fuel[23] or its elemental composition and the devolatilization temperature[24]. The representative primary tar species used include oxygenated hydrocarbons, such as acetol ($C_3H_6O_2$), catechol ($C_6H_6O_2$), and vanillin ($C_8H_8O_3$), which are converted to secondary tar species, such as toluene, phenols, and intermediate species. In the model of Fuentes-Cano *et al.*[24], all these species contribute to the subsequent formation of naphthalene and benzene, which, in turn, form the larger tertiary tar (pyrene) and soot. In the model of Font Palma[23], benzene is formed from catechol or the conversion of naphthalene, and all the heavier tar species are formed through polymerization reactions that involve catechol and cyclopentadiene, which is generated during the conversion of phenol. With the exception of the formation of benzene from naphthalene, neither of the two models allows reactions that generate smaller aromatic species from larger species, as reported previously[25, 27, 30, 31].

In Paper 6, the SPA-tar spectrum described in Papers 1 and 2 was complemented by additional model compounds, so as to describe more accurately the behaviors of furans and species that contain four aromatic rings. In addition, the unknown species in the SPA-tar were distributed between the other groups of pure hydrocarbons (according to boiling point), and

UCS were used to describe the primary tar and intermediate species that can affect the formation of SPA-tar. Consequently, the SPA-tar and UCS were categorized into groups according to size and level of maturation. The SPA-tar group was subdivided into the following eight groups [with the representative species in parentheses]: phenolic species [phenol]; furans [2,3-benzofuran]; benzene; 1-ring aromatic species with branches [toluene]; naphthalene; 2-ring aromatic species with branches [acenaphthylene]; 3-ring aromatic species [phenanthrene]; and ≥4-ring aromatic species [pyrene]. The UCS were divided into the abovementioned pseudo-components of formic acid and butane (F and B), and the secondary species F′ and B′ were employed to facilitate two levels of reactivity of the UCS. In other words, while some UCS will form SPA-tar and cold gas directly, some will generate secondary UCS (UCS′) which, in turn, can form SPA-tar and gas. Therefore, the experimental data for UCS are assigned as secondary UCS, while the primary species are considered to attain the measured UCS levels twice as fast as the secondary UCS (i.e., in half the residence time).

The reaction scheme developed in Paper 6 is based on findings reported previously[2, 23-26] and includes the contribution of the determined UCS. Thus, the formation of SPA-tar can be described using a known parameter, while satisfying the mass balance of the system. The scheme should comply with the order of maturation described by Milne *et al.*[2], whereby the CS evolve from oxygenated to aromatic species. Furthermore, it should take into account the reactions associated with mature tar[25, 26], in which multiple-ring species can either dissociate into smaller aromatic species or form even larger species, approaching soot. In line with previous studies[22-24], the UCS are considered to form simple tar species, such as phenols, toluene, and UCS′ which, in turn, can form more complex species. Furthermore, as the UCS′ are considered to contain species (e.g., cyclopentadiene) that are known to partake in polymerization reactions that yield both pure and branched poly-aromatic species (R3), the scheme also accounts for the formation of mature components from UCS′. Nevertheless, these reaction routes are somewhat suppressed in favor of the remaining routes when deriving the reaction scheme, so as not to undermine the concept of tar evolution. The main assumptions concerning the proposed scheme are that: (1) all CS are initially found as primary UCS: (2) SPA-tar is formed *via* reactions of UCS, UCS′ or other SPA-tar species with a carbon yield lower than unity; and (3) oxygen cannot be added to the CS, it can only be transferred from species that already contain oxygen (UCS, phenols, and furans).

In addition to the various employed reaction schemes, several alternative reaction expressions have been proposed[25-28, 32]. The types of reactions used for tar include thermal dissociation reactions that are dependent on the level of the species of interest[25], as well as hydrogenation, polymerization, and heterogeneous reactions[23, 32, 53]. For experimentally determined reaction kinetics, the reaction rate expressions are defined as a function of reactant concentration (C), and temperature (T):

$$r = f(C, T) \tag{10}$$

In the case of controlled, dedicated experiments, the determined rate expressions can be highly accurate, while the kinetic data derived from larger systems with unknown fluctuations will have associated uncertainties. Consequently, uncertainties related to, for example, the temperature of the system will be reflected in the derived rate coefficients, turning them into lumps that encompass several unknown parameters, so as to ensure a satisfactory global reaction rate that is proportional to the perceived temperature. Paper 6 is limited to proposing a general reaction scheme for CS, and the obtained measurements were used to derive these types of lumped kinetic coefficients. Consequently, the derived rate coefficients are referred to as 'relative rate coefficients', to emphasize that they are limited to describing the dynamics of the investigated system in proportion to the perceived process parameters. The reactivity of each modeled group or species (i) is described through three global reaction rates that cover thermal dissociation and reactions with steam and hydrogen:

$$r_i = -C_i * k_{1,T,i} * e^{-\left(\frac{k_{2,T,i}}{T}\right)} - C_i * C_{H_2O}^{x} * k_{1,H_2O,i} * e^{-\left(\frac{k_{2,H_2O,i}}{T}\right)} - C_i * C_{H_2}^{y} * k_{1,H_2,i} * e^{-\left(\frac{k_{2,H_2,i}}{T}\right)} \quad (11)$$

where C denotes the concentration [moles/m^3], x and y are the reaction orders of steam and hydrogen, respectively, and the constants k_1 and k_2 represent the relative rate coefficients. The use of the three global reactions takes into account the effects of the temperature, steam, and hydrogen concentrations. This, together with the use of relative rate coefficients, ensures that the model is sufficiently flexible to describe the behavior of the studied system. Regardless of which individual types of reactions control the maturation of tar, the sum total of the proposed reactions for any species should generate a reasonable overall reaction rate.

Additional factors that affect the reaction rate expressions, such as the effect of bed material aging, the extent of gas-particle interactions, and the catalytic effects of ash components (such as alkali)[54, 55], are probably needed to explain fully the reaction rate of any given species. While evaluation of the effects of catalytic components is outside the scope of Paper 6, earlier and parallel studies have indicated that it is an important parameter for the evolution of tar[56]. Therefore, if the levels of catalytic components are constant throughout the measurements employed in Paper 6, their effects will be included in the various *k*-values of Eq. (11), although variations in the levels of catalytic activity will not be taken into consideration. It should be mentioned that on-line measurement systems for the quantification of alkali species have been presented previously[57].

3 - Experimental Equipment

Several different reactor and measurement systems have been employed and developed within the framework of this thesis. The following sections describe the design and general operation of the relevant equipment, as well as the modifications made during the work.

3.1 Gasifier and Measurement Systems

The gasifier measurements were performed in the Chalmers 2–4-MW DFB gasifier, depicted in Figure 8. In this system, the unconverted fuel from the gasifier is combusted together with additional fuel and the bed material in the CFB boiler (1). The hot bed material is separated from the flue gas in a cyclone (2), after which it enters the particle distributor (4). The flue gas exits at the top of the cyclone and continues towards a series of heat exchangers (3). When the system is operated as a boiler, the bed material exits the particle distributor and returns directly to the boiler. When the system is operated as a DFB gasifier, the hot bed material flow is redirected to the gasifier (5), where it provides the heat necessary for gasification reactions. The cooled bed material exits the gasifier together with the unconverted fuel and char and subsequently enters the boiler. Two separate fuel feeding systems (6) are used for the boiler and gasifier. The produced raw gas, exiting the gasifier, is transported to the boiler for combustion. All performed gas measurements are performed on a slipstream of gas, which is extracted from the sample collection point of the raw gas channel (x).

During measurements, the gasifier is fluidized using steam that contains a known amount of helium, usually at 20–50 Nl/min, to allow the quantification of gaseous species[45]. The helium is added to the steam prior to introduction into the gasifier to facilitate an even distribution throughout the gasifier. The resulting volumetric fraction of helium in the cold gas is around 0.5%–1.0%. The gasifier is operated with wood pellets at 1–2 kPa sub-atmospheric pressure and a temperature of around 820°C.

The instrumental setup for gas analysis after the HTR (as used in Paper 4) is depicted in the left panel of Figure 9. Raw gas (1) is continuously sampled through a heated ceramic filter (2), which is maintained at 350°C and used to remove particles from the gas before it enters the HTR (3). Samples for the SPA analysis are collected directly at the outlet of the HTR (4), as described in Paper 3, to determine the degree of reformation of the SPA-detectable tar fraction. The gas flow is cooled and the steam is condensed in a Peltier cooler (5), after which the aerosols are separated using a filter (6). The dry gas is passed through a pump (7) and a flow meter (8) before reaching the micro-GC (9).

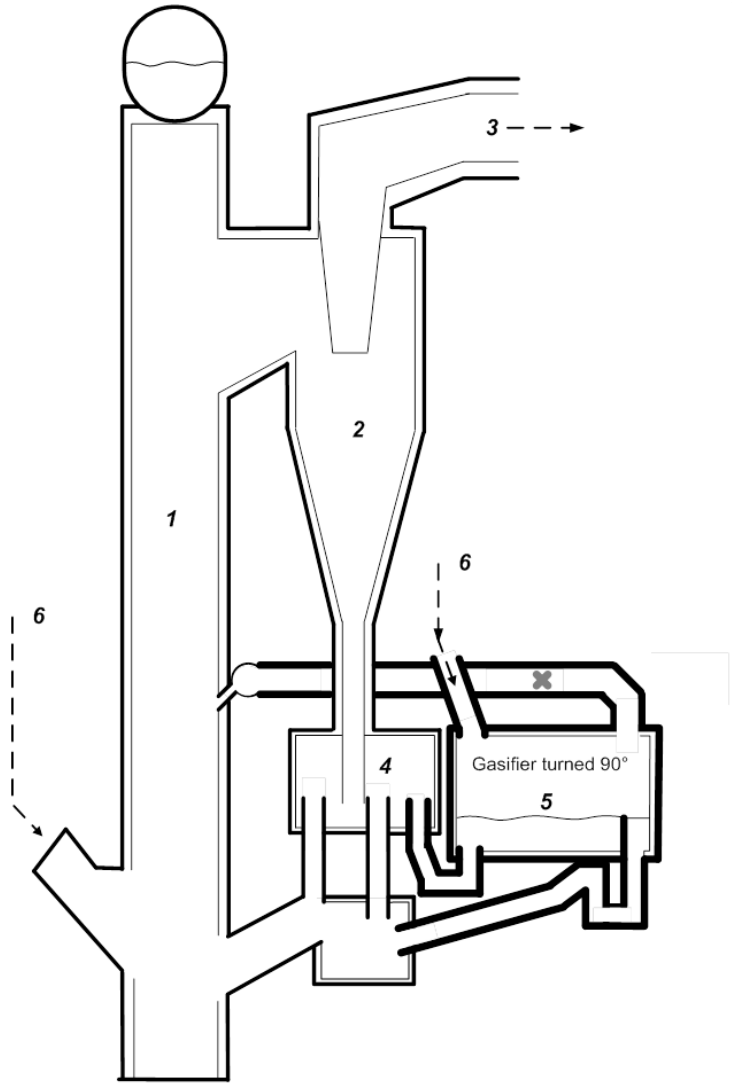

Figure 8: Schematic of the Chalmers DFB gasifier system showing the: 1, CFB boiler; 2, cyclone; 3, flue gas path; 4, particle distributor; 5, gasifier; and 6, fuel feeding systems.

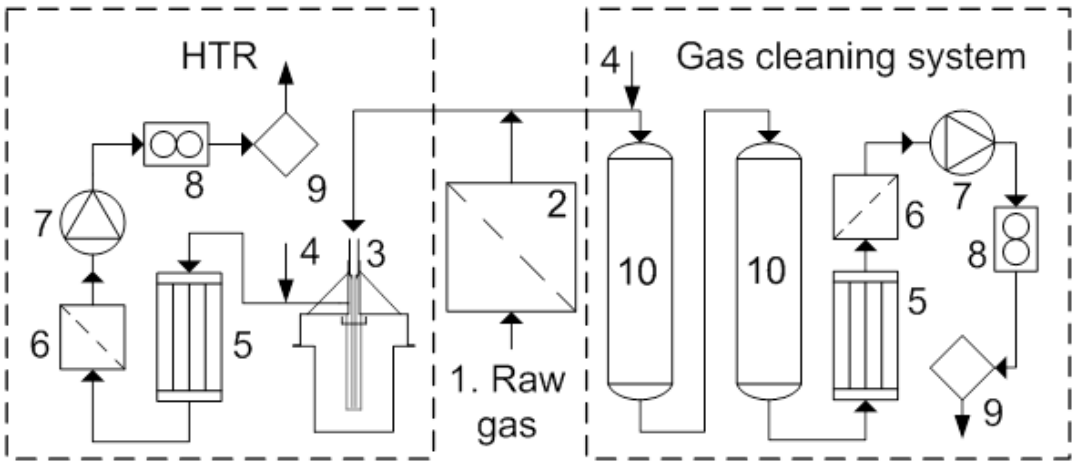

Figure 9: Schematics of the HTR system (left) and the gas-cleaning system (right). The identified features are the: 1, raw gas from the gasifier; 2, ceramic filter; 3, HTR; 4, SPA sampling point; 5, Peltier cooler; 6, filter; 7, gas pump; 8, flow meter; 9, micro-GC; 10, coolers.

Cold gas measurements are performed on the untreated raw gas, using the gas cleaning system (right panel in Figure 9) to determine the dry raw gas composition, concentration of steam, and amount of tar. SPA samples (4) are collected directly after the ceramic filter (2), after which the gas is quenched with isopropanol in two coolers (10), which condense the tar and steam. The gas is further cooled in a Peltier cooler (5), after which it passes through a wool filter (6), to separate the aerosols, a pump (7) and a flow meter (8), before being analyzed in the micro-GC and NDIR instrument (9).

The SPA sampling point (4) of the gas cleaning system was constructed as depicted in the left panel of Figure 10. During measurements, roughly 2 Nl/min of dry raw gas is transported through a heated gas line (350°C), followed by a volume that is heated to the same temperature before reaching the quenching point. The heated volume (350°C) is equipped with a septum that is mounted a short distance from the wall to avoid melting, and this serves as the entry point for the sampling syringe. The SPA samples are collected by attaching an SPA column to a 100-ml syringe *via* a universal tube connector, inserting the needle (1.2×50 mm) into the hot gas flow *via* the septum, and extracting 100 ml of gas through the column using the syringe. The remaining raw gas continues through to the quench, after which it is cooled and dried before it reaches the online gas analysis equipment. The relatively small flow of gas and the positioning of the quench were selected to ensure a strong response in the N_2 and O_2 concentrations if a leakage should occur during sampling.

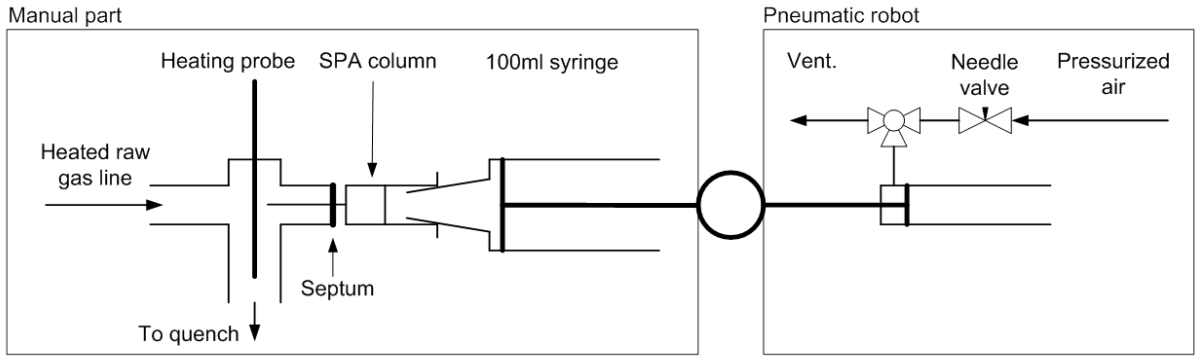

Figure 10: Left panel: the SPA sample point, SPA column, and manual part of the extraction device. Right panel: the pneumatic device used for consistent sample extraction.

The 100-ml syringe is operated by a pneumatic device during sample extraction, to ensure reproducible sampling (right panel, Fig. 10). The device consists of a pneumatic cylinder, connected to the syringe, which is filled with pressurized air at a flow rate that is regulated by a needle valve. This flow rate was calibrated to allow sample extraction times of 1 minute. After collection of a sample, the pressure in the cylinder is released. If a blockage in the needle results in the formation of a vacuum, the syringe piston will retract. When this happens the column is discarded and replaced.

The two gas chromatographs used for SPA-tar analysis, the BRUKER GC-430 and GC-450, were operated in the split mode using the SGE 4-mm FocusLiner with fused silica wool, autosamplers, FID detectors, and mid-polar BR-17-ms columns with graphite ferrules. The different species used to calibrate the gas chromatographs are presented in Paper 3. The temperature ramp, from 50°C to 350°C, was developed to measure components ranging from benzene to coronene. The injector and detector temperatures were set at 350°C, the split ratio was 20, and the column flow was set to 1 ml/min with helium as the carrier gas. The oven was programmed to hold at 50°C for 5 minutes, after which the temperature was increased by 8°C/min until 350°C was reached, and this temperature was maintained for an additional 12.5 minutes to ensure that the entire tar spectrum was retained. This setup gave a reproducibility level that was within 5% for each chromatograph. During the sample analysis, each sample vial was analyzed three times sequentially, after which the mean values for all the peaks were calculated.

3.2 CLR Reactor System

The CLR reactor is depicted in Figure 11 together with auxiliary systems, such as the analysis equipment and gas supply systems. The employed reactor and analysis systems are thoroughly described elsewhere[8], as well as in Paper 1, and can be summarized as follows. Raw gas is introduced to the fuel reactor (FR), which contains a bubbling fluidized bed (indicated in the figure). The reformed gas exits at the top of the FR, where SPA samples are collected before the gas is conditioned and subsequently analyzed. The air reactor (AR) contains a circulating fluidized bed in which the bed material is regenerated by a mixture of air and nitrogen. Similarly to the FR, the spent air flow is conditioned and analyzed after exiting the reactor. The FR and AR are separated by two loop seals, which prevent the exchange of gas between the reactors and which are fluidized with helium. The use of a different gas in the seals, such as argon or steam, would contribute to closing the mass balance of the system. Nevertheless, the measurements performed describe clear trends for the concentration and composition of the measured tar.

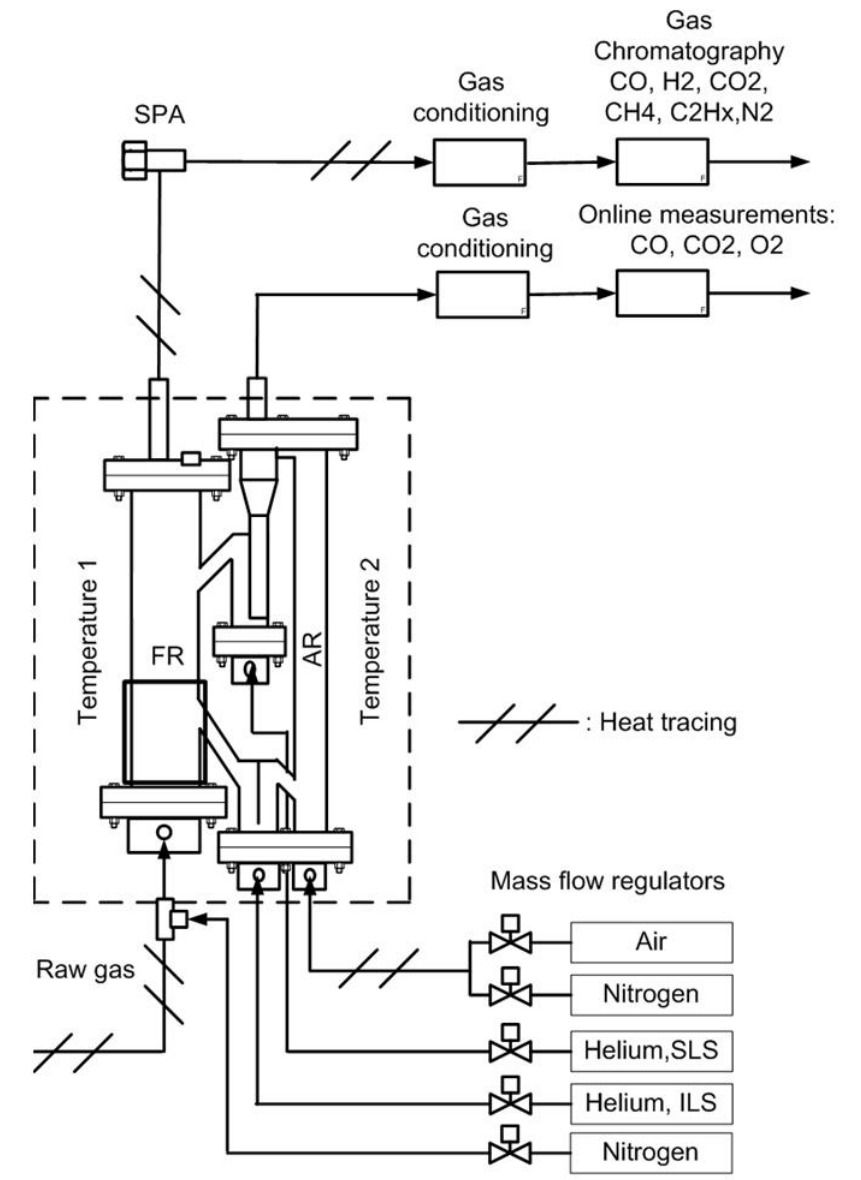

Figure 11: Schematic of the CLR setup.

3.3 High-Temperature Reactor System

The HTR described in Paper 4 (left and middle schematics of Figure 12) consists of a ceramic reactor and oven located inside a gas-tight steel casing. Gas, at a temperature of 350°C, is introduced to the top of the reactor *via* a stainless steel adaptor (1). The adaptor is connected to the reactor by a flange (2) using graphite packing to avoid leaks. The other end of the adaptor is connected to an 8-mm alumina (Al_2O_3) tube (3) using a stainless steel fitting with graphite packing, to create a leakage-free joint without breaking the alumina tube. The lower part of the reactor contains a larger 35-mm alumina tube with a closed bottom (4), surrounded by four heating elements (5) (Kanthal Super 1800). The top part of this tube is connected to the reactor ceiling using a pack box (6) with graphite packing. The outer shell of the reactor is composed of stainless steel and is designed to be gas-tight at operational pressures (80–101 kPa). In the event of excessive internal gas exchange between the large alumina tube and oven, the gas in the oven can be continuously evacuated to ensure minimal back-mixing into

the reactor. During operation, gas is drawn through the adaptor and is heated during its transport to the bottom section *via* the narrow alumina tube. The narrow tube ensures minimal residence times at temperatures that promote high yields of soot but that are too low to support soot gasification. The gas then enters the larger alumina tube and is slowly transported upwards through the high-temperature section of the reactor. The gas exits the reactor *via* an outlet (7) that is positioned 10 cm below the inlet adaptor to avoid excessive convective heating of the upper graphite packing.

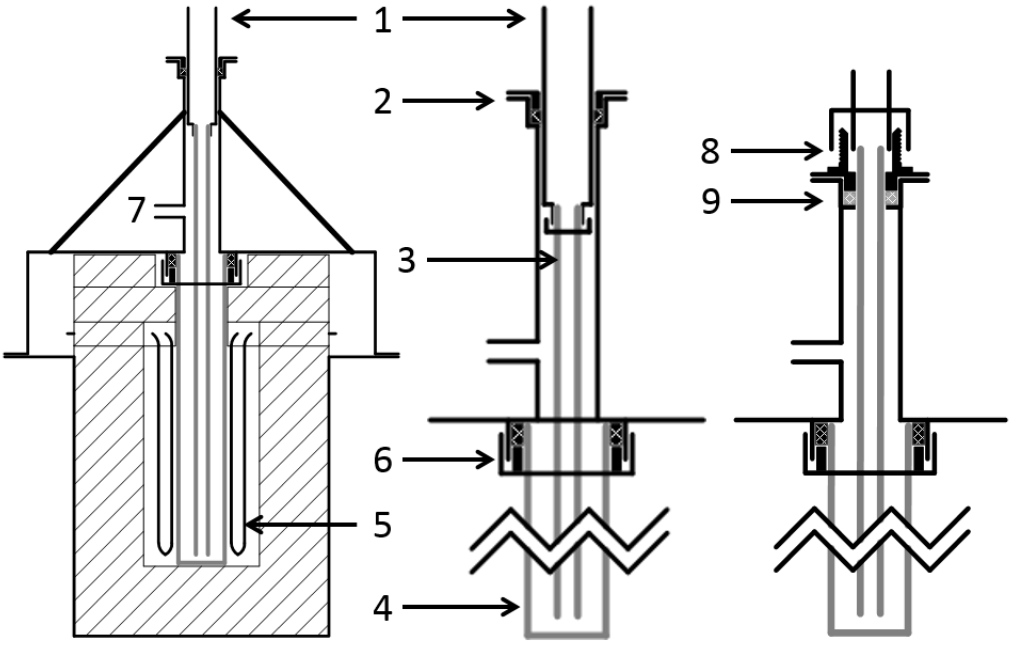

Figure 12: Schematic of the high-temperature reactor used in Paper 4 (left), with an enlarged image of the connections (middle). The reconfigured version (right) was used in Papers 5 and 6.

The inlet connections (2) of the HTR used in Paper 4 (Fig. 12) were found to be prone to leakage caused by mechanical stress, resulting in small volumes of air entering the reactor and gas bypassing the reactor. Furthermore, the adaptor (1) that held the thin alumina tube (3) exhibited sideways movement, causing this tube to be pushed against the wall of the larger alumina tube (4) to the point of breakage. Consequently, the inlet of the reactor was modified (right schematic of Fig. 12) to ensure a gas-tight seal with good mechanical properties. Here, instead of using an adaptor, the thin alumina tube (3) is connected directly to the pack box using graphite packing (9), to minimize movement and contact with the larger alumina tube (4). In addition, the top flange of the pack box is fitted with a male connector (8) of sufficient diameter (14 mm) to ensure that the connecting tube can envelop the thin alumina tube without coming into contact with it. With this design, neither the packing nor the alumina tubes are affected by outside forces, thereby minimizing the risks of leaks and breakages.

4 - Methodology

The following section describes the experimental and theoretical methodologies employed throughout Papers 1–6.

4.1 CLR Operation

The effects of varying temperatures and levels of oxygen in the air reactor are investigated in Paper 1, for a bed material composed of silica sand and 23% manganese oxide. During the measurements, the gasifier was operated at bed temperatures of approximately 825°–830°C and the CLR was operated at 700°C and 800°C. Furthermore, the concentration of oxygen in the air reactor was varied between 1.0% and 2.2% for both temperatures of operation.

4.2 Gasifier Operation using Ilmenite

Paper 2 describes the effects of different levels of ilmenite in the bed material (silica sand) on the raw gas produced in the Chalmers DFB system. The gasifier was operated with wood pellets and ilmenite fractions in the range of 0%–12% of the bed material. Measurements were performed at high and low levels of fluidization for all the investigated percentages of ilmenite to discern the effects of increased gas-solid contact. The remaining operating parameters of the gasifier were kept as constant as possible across the different measurements. As a result, the average bed and gas temperatures were in the range of 821°–833°C and 788°–801°C, respectively. However, due to the different levels of fluidization, the steam-to-fuel ratio and average gas residence time were in the range of 0.81–0.82 $kg/kg_{daf\ fuel}$ and 3.87–3.96 s respectively, for low-level fluidization, and 1.06–1.07 $kg/kg_{daf\ fuel}$ and 3.25–3.36 s, respectively, for high-level fluidization. Consequently, the effects of changes in residence time and steam concentration are present in addition to the effects of increased gas-solid contact.

4.3 Evaluation of the SPA Methodology

Paper 3 investigates the reproducibility of the SPA method, as well as its sensitivity to the effects of inappropriate sample collection and subsequent treatment. The measurements performed consisted of six SPA columns each, collected within a time period of about 10 minutes. The columns, with the needles still attached, were then sealed and stored in a freezer, to minimize desorption of the more volatile components, after which the columns were eluted within 24 hours of sampling.

The elution of the collected SPA samples in the studies reported in Papers 1, 2, and 3 was performed as described in Paper 3. However, in light of the findings of Paper 3, the elution procedure was re-evaluated and recent measurements have been conducted as follows. Only one solvent and one internal standard are used, with the solvent consisting of a mixture of eight parts dichloromethane (DCM), one part isopropanol (IPA), and one part acetonitrile (ACN), and the internal standard being 4-ethoxyphenol. During elution, the needle is flushed with 0.5 ml of solvent that is deposited on the top of the column, after which a weak flow of nitrogen is used to push the solvent through the column. The internal standard is added directly to the vial, after which an additional 1.5 ml of solvent is flushed through the column. This procedure is repeated for all the columns, with the exception of flushing the needle, to obtain a control sample, which serves both to evaluate and enhance the elution.

A series of eight SPA measurements, each resulting in four to six usable columns depending on the success of the sample collection, was collected for different operating modes of the gasifier to obtain a wide range of tar yields and compositions. These samples were analyzed to determine the behaviors of the heaviest detectable tars, such as coronene. As mentioned above, a temperature of 350°C was maintained in all the heated pipes and equipment to avoid condensation. Furthermore, measurements and visual inspection of the transfer lines were performed to ensure that no condensation had occurred.

To determine the reproducibility of the method, the tar spectrum was divided into the known compounds and groups of unknown species that exited the chromatographic column between two known compounds, being lumped together as one value. The relative standard deviations (%RSD) were calculated for each group and known compound in each SPA measurement and were compared to the corresponding collected mass fractions.

4.4 Evaluation of the High-Temperature Reactor System

Synthetic gas HTR measurements were performed to determine the overall degree of conversion and soot formation in the reactor. The start-up procedure for the measurements involved initiating a temperature ramp a few hours before operation, to allow the alumina tubes to heat up slowly, thereby avoiding cracking as a result of thermal expansion. When the operational temperature was reached, the reactor was purged with nitrogen before starting the measurement. Synthetic gas of a known composition was supplied from a gas bottle and mixed with steam to 50%vol before entering the reactor. After the reactor, soot particles were collected in an uncoated diesel particulate filter (DPF), which was maintained at 150°C during the operation. The particle-free gas was then cooled to condense the remaining steam before it was analyzed in a Varian CP4900 micro-GC[45], which was capable of analyzing all the species in the supplied gas. The collected soot was quantified at the end of each measurement by introducing a known flow of air into the system while maintaining the reactor temperature. The oxidation of the system was performed at an initial filter temperature of 150°C, to separate the combustion of remaining gas and soot attached to the pipe walls from the soot captured by the filter. Due to the rapid combustion of the soot, the levels of produced CO and CO_2 were measured using an NDIR instrument (Rosemount MLT) to gather data once per

second. Once a stable, atmospheric CO_2 background was obtained, the filter temperature was increased to >500°C, to allow combustion. As a result, the quantified levels of soot should be considered indicative of the total soot yield. Soot formation was determined at temperatures of 1500°C, 1600°C, and 1700°C. Furthermore, the measurement at 1700°C was used to determine the stability, accuracy, and reproducibility of the reactor system.

4.5 Applied High-Temperature Reactor Measurements

The HTR gasifier measurements were performed in parallel with the gas cleaning system in the Chalmers DFB gasifier according to the scheme in Figure 9. During the measurement, the gasifier was operated with bauxite as the bed material to determine aging effects in a separate study. As a result, the system exhibited significant char conversion and oxygen transport between the boiler and gasifier. SPA samples were collected directly after the reactor, to ensure complete conversion of the measurable tar components, and prior to the gas conditioning system to allow analysis of the tar, as well as the UCS.

The performance of the system was monitored during the measurements to detect possible errors, including air leakages into hot zones, escape of soot from the HTR, and incorrect synchronization of the equipment. Leakages of air prior to the HTR may be interpreted as oxygen addition, as the leaked air is combusted. Therefore, the He/N_2 ratios of the cold gas and the HTR gas were monitored for any deviations. When detected, the amount of leaked air could be determined, and compensated for, by comparing the nitrogen flows of the two systems. The escape of soot from the HTR affects the determined fuel conversion, as well as the yield of condensable compounds. Thus, complete soot conversion needs to be guaranteed for reliable measurements. Incorrect synchronization of the measurements can further complicate the analysis of transient measurements. However, this is rarely a problem as the initiation of helium provides the difference in response time for the two systems.

4.6 Parameter Study for DFB Systems

In light of the findings reported in previous papers, the measurements for Paper 5 were carried out with the aim of describing the effects of various process parameters based on a complete mass balance. To this end, the reconfigured HTR (right side of Figure 12) was employed, together with the extended version of the SPA method, which enabled improved quantification of the BTX species. This extension consisted of two sample extraction columns that contained a secondary bed of active carbon, as proposed by Osipovs[47], in addition to six columns with only 500 mg of aminopropyl-bonded silica adsorbent. This allowed for more accurate quantification of all the tar species, which ranged from benzene to coronene, and served to compare the two types of sample extraction columns used.

The investigated parameters consisted of the average raw gas temperature, the level of fluidization (the steam-to-fuel ratio), and the residence time at a constant steam-to-fuel ratio when using silica sand as the bed material. The process parameters used for the investigated cases are summarized in Table 2, which also lists (in parentheses) the recalculated values used in Paper 6 (described below). The average gas temperature for Paper 5 was calculated as the

average value between the bed temperature and raw gas temperature (described by Larsson *et al.*[45]), and this was also used to determine the gas residence time. It should be noted that the determined average gas temperature does not necessarily constitute a representative temperature of the volatile gases, and that the "true" representative temperature may be quite different. Nevertheless, it offers a consistent way to describe the differences in gas temperatures between different experiments. The gas residence time in the freeboard of the gasifier was calculated using the volumetric flowrate, exiting the gasifier, at the average gas temperature. Consequently, the determined values are likely to be lower than the actual residence times but are still useful for describing the differences between the experiments. The steam-to-fuel ratio was calculated as the sum of all the steam entering the gasifier from the loop seals, the fluidization steam, and the moisture of the fuel divided by the dry, ash-free fuel feed. The measurement names in the first column also contain the relevant value of the parameter of interest, to facilitate identification in later figures.

Table 2: Summary of process parameters for the experiments performed in Paper 5; alternative values for the average gas temperatures and residence times used in Paper 6 are shown in parentheses.

Measurement name	$T_{avg, bed}$ [ºC]	$T_{avg, gas}$ [°C]	Fuel [kg/h]	Steam [kg/h]	Steam-to-fuel ratio [kg/kg_{daf}]	Residence time [s]
High T (T774)	823	774 (792)	294	160	0.87	4.65 (4.72)
Medium T (T758)	804	758 (774)	294	160	0.87	4.77 (4.90)
Low T (T744)	786	744 (758)	295	160	0.86	4.89 (5.07)
High steam (S190)	811	767 (783)	295	190	0.98	4.43 (4.52)
Medium steam (S160)	811	764 (781)	294	160	0.87	4.74 (4.86)
Low steam (S130)	813	761 (779)	295	130	0.75	5.09 (5.19)
Long residence time (R5.49)	809	754 (773)	252	130	0.86	5.49 (5.61)
Medium residence time (R4.24)	801	758 (773)	338	190	0.86	4.24 (4.31)
Short residence time (R3.95)	799	758 (772)	369	210	0.85	3.95 (4.01)

4.7 Deriving a Reaction Scheme for Condensable Species

The values for the average raw gas temperatures used in Paper 6 differ somewhat from those in Paper 5 because a distant temperature measurement was excluded to obtain a more representative value of T_{avg}. As a result, T_{avg} was determined as the average of the mean bed temperature and the outlet raw gas temperature. This, together with minor changes in the calculations of the molar flow rate, affected slightly the determined residence time. The question as to whether the determined values for the temperature and residence time are

reliable for describing the gasifier remains important. Nevertheless, assuming that the errors in temperature and residence time are similar for all the cases, the generated data are sufficient to match the purposes of Paper 6.

The collected experimental data-points were compared to the same starting point for the purpose of deriving the reaction pathways. The employed starting point was adopted from Neves *et al.*[44] and was derived for pyrolysis of a similar fuel (wood pellets) at 600°C. The main assumption linked to the usage of this measurement as the starting point is that the gas composition of all the performed measurements at one point in time resembles that of the pyrolysis time-point. Consequently, all the modeled cases originate from the point of pyrolysis at 600°C and evolve over a timespan that reflects the difference in residence time between the pyrolysis point (set at 3 seconds)[44] and the gasification points. At the starting point, the amount of SPA-tar is assumed to be zero, while all the carbon found in the CS is designated as UCS, resulting in yields for F and B of 8.0 and 2.8 mole/$kg_{daf,\ fuel}$, respectively. Furthermore, as all the cases exhibit different volumetric flow rates and temperatures, the starting concentrations of UCS (in moles/m^3) will vary. The actual starting yields of F and B most likely varies for the different cases due to e.g. the varying temperature of the gasifier. However, considering the uncertainties related to other parameters, such as temperature and residence time, assuming constant yields of F and B is acceptable for the purpose of this work.

In the proposed model, UCS are formed only during the primary pyrolysis and are not affected by any other tar species. This allows the conversion reactions of UCS, UCS′, and phenol to be solved analytically, provided that they are solved in sequence, as UCS′ are dependent only upon the conversion of UCS, while phenol is dependent upon the conversion of both UCS and UCS′. As a result, the exponents x and y in Eq. (11) can be obtained at a reasonably low computational cost, assuming that they are identical for the reactions of all the groups, and initial values for the solver are generated. Furthermore, this offers an efficient means for assessing whether the measurements follow sufficiently uniform trends to allow a good fit. It is well known from previous experience with the examined system that aging of the bed material and other unquantified factors can drastically alter the gasifier performance[5]. This means that measurement points that do not comply with the major trends must be excluded and subsequently compared with the final model to assess the severity of the deviation.

As described in Paper 6, the solver randomly generates the distribution and relative rate coefficients (based on the initial values from the analytical solution), simulates all the measurements, and calculates the total error. This procedure is then repeated, based on the values of the simulation that resulted in the smallest error, until a reasonably good fit is obtained. The resulting model, which describes the tar evolution, should be capable of presenting realistic trends for the amount and composition of the tar. However, due to the uncertainties related to the temperature and residence time, as well as those associated with describing the gasifier as a plug flow reactor, the predicted rate of change within the system will be approximate. Consequently, Paper 6 should not be viewed as a kinetic study, but

rather as an attempt to map the routes by which mass is transferred through the various groups during the maturation of the tar.

5 - Results & Discussion

The following results are presented so as to parallel the structure established in the *Introduction*, and can be regarded as three different parts of the work conducted within this thesis. The first part, which is concerned with the primary and secondary measures for tar reduction, highlights the importance of understanding the differences in catalyst performance that can be caused by its implementation. However, it also emphasizes the importance of quantitative measurements to obtain a clear description of the behavior of the raw gas. The aim of the second part of the work is to develop and refine the performed measurements to allow a comprehensive overview of all the aspects relevant to the fuel conversion. Ultimately, in the third part, the derived measurements are implemented to identify trends for previously unquantified phenomena and to create an updated view of the gasifier performance. This, in turn, can serve as the basis for further development of the employed measurement systems.

5.1 Secondary Measures

The measured concentrations of tar (g/Nm^3) that exit the gasifier and CLR are depicted in Figures 13 and 14 for operating temperatures of 700°C and 800°C, respectively. The measured tar spectrum is divided into the subgroups of: phenols; benzene, 1-ring aromatic species with branches; naphthalene; 2-ring aromatic species with branches; 3- and 4-ring aromatic species; and unknown components. However, as previously stated, the measurement of benzene in Papers 1–4 is unreliable, such that no conclusions can be drawn from its behavior. For both operating temperatures, the catalytic activity increases as additional oxygen is introduced into the air reactor. This increase may be due to higher levels of oxygen transport, resulting in combustion, although it could also be due to more extensive regeneration of active surfaces on the catalyst[41]. Overall, the changes in tar composition attributed to increased severity in terms of temperature and catalyst activity resemble those reported for other bed materials, such as ilmenite[8]. The concentrations of phenols, branched 1- and 2-ring species, and unknown species decrease throughout the experiments shown in Figures 13 and 14 due to increased severity. In contrast, the concentrations of naphthalene and 3- and 4-ring species initially increase due to polymerization of other tar species and lighter gas components. At 800°C and 2.2% O_2 in the AR, the levels of the 3- and 4-ring species start to decrease and the increase in naphthalene slows, which indicates that a further decrease can be expected at higher temperatures and higher levels of catalyst regeneration.

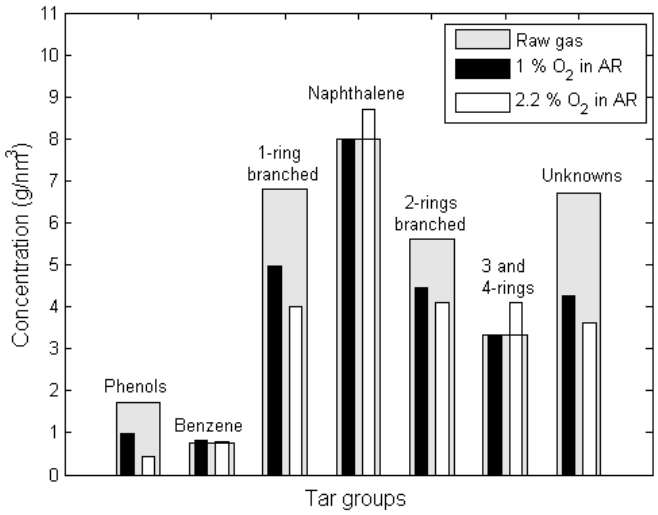

Figure 13: Tar compositions of the raw gas and reformed gas at 700°C.

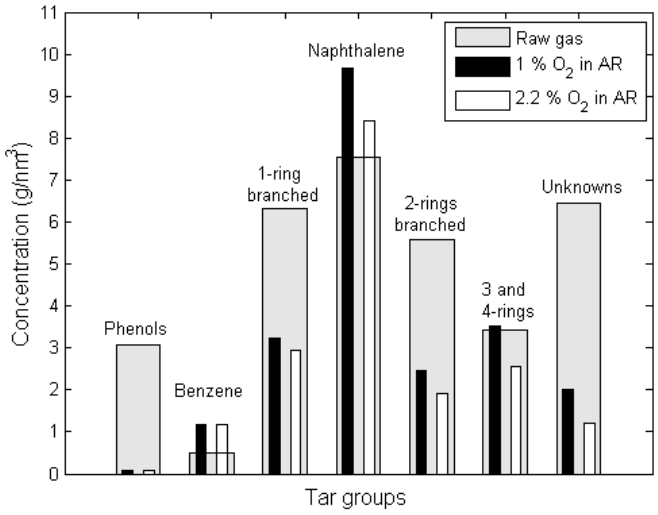

Figure 14: Tar compositions of the raw gas and reformed gas at 800°C.

5.2 Primary Measures

The gasifier was operated at two different levels of fluidization with ilmenite fractions ranging from 0% to 12% in the bed. The measured tar concentrations are depicted in Figures 15 and 16, similar to those observed for the CLR measurements, for low and high levels of fluidization, respectively. The reference cases, in which silica sand was used as the bed material, are similar to those of the CLR operation. However, the trends for changes in the tar composition due to increased severity resemble neither the CLR measurements nor the expected trends of tar maturation according to Elliott (Fig. 4). Instead of shifting the compositions, the measurements performed at low fluidization (Fig. 15) simply show decreases in the concentrations of all groups, although the phenols seem to be affected to a lesser degree than the other compounds. Furthermore, as shown in Figures 17 and 18, this is not an effect of dilution because the calculated yields of tar species follow the same trend.

Presumably, at low levels of fluidization, the degree of contact between the gases and solids in the freeboard of the gasifier is limited. Consequently, the decrease in tar is attributed to a high level of contact between the devolatilizing fuel particles and the surrounding bed material. This results in the reformation, or oxidization, of the newly formed primary tar species. The fraction of primary tar that is able to avoid contact with the active material subsequently matures in line with the pattern observed for normal (silica sand) operation of the gasifier.

At higher levels of fluidization (Fig. 16), the tar composition deviates significantly from the expected trend. The concentrations of both phenols and unknown species are increased, which indicates that the conditions in the gasifier are less severe, since these species are rather easily reformed. This suggests that the effects of a shorter residence time outweigh the effects of increased gas-solid contact. However, as stated in Paper 2, the high level of fluidization also results in higher yields of heavy tar species, indicating increased polymerization due to increased severity. The explanation for these effects could perhaps lie in the behavior of the UCS, although the measurements described in Paper 2 do not yield this information. Nevertheless, the measurements performed in the gasifier, compared to those in the CLR, show that the performance of a catalytic material is strongly dependent upon the mode of implementation.

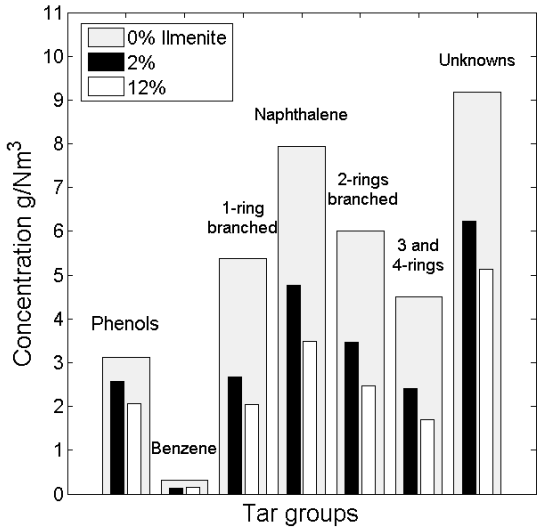

Figure 15: Tar compositions for low levels of gasifier fluidization with 0%–12% ilmenite in the bed.

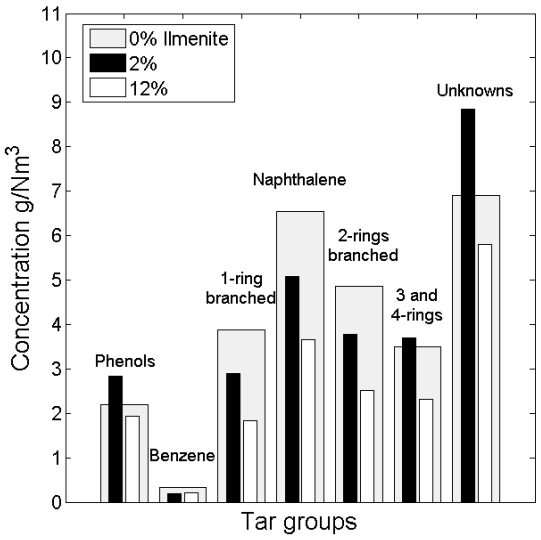

Figure 16: Tar compositions for high levels of gasifier fluidization with 0%–12% ilmenite in the bed.

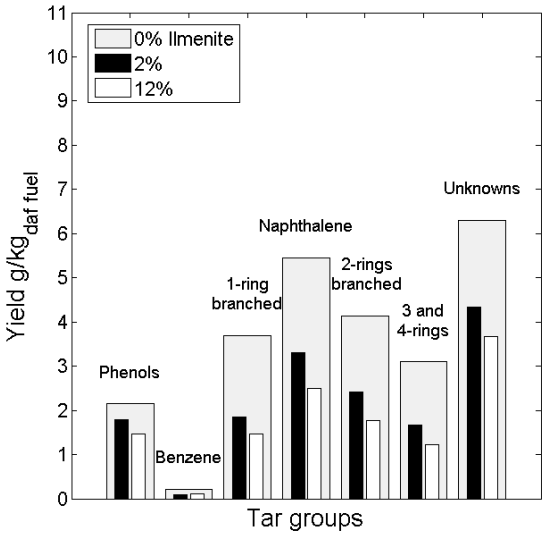

Figure 17: Tar yields [g/kg$_{daf\ fuel}$] for low levels of gasifier fluidization with 0%–12% ilmenite in the bed.

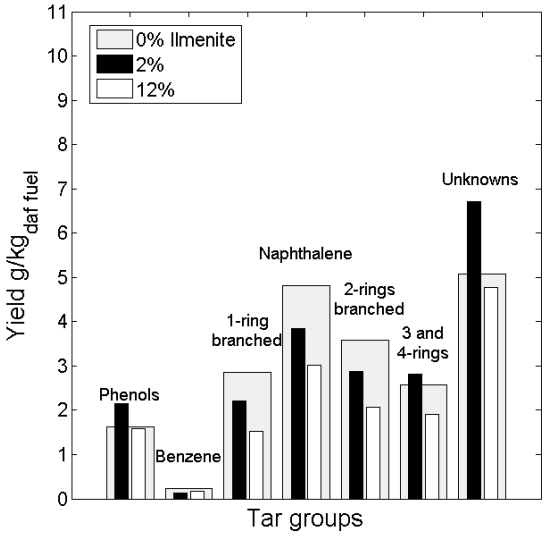

Figure 18: Tar yields [g/kg$_{daf\ fuel}$] for high levels of gasifier fluidization with 0%–12% ilmenite in the bed.

Overall, the reduced levels of tar seen for CLR operation at 800°C and for low levels of gasifier fluidization with 12% ilmenite in the bed are comparable. However, the cost associated with these reduction, in terms of oxygen transfer, differs greatly. Figure 19 shows the molar H/C- and O/C-ratios of the measured fractions of CO, CO_2, and H_2 in the cold gas for the gasifier measurements, using 0% and 12% ilmenite at high and low levels of fluidization, as well as the CLR measurements at 800°C with 1.0% and 2.2% oxygen in the AR. The solid line, which originates from the point of low fluidization with only silica sand, indicates the change in the H/C-ratio as a function of the WGSR. With the exception of high levels of fluidization with silica sand, all the points are below the line of the WGSR due to oxygen transport. However, the oxygen transport is significantly weaker for the CLR measurements than for the measurements performed in the gasifier, particularly with 1% O_2 in the AR. Furthermore, the potential for minimizing the oxygen transport in the CLR is greater than in the gasifier, as it is decoupled from the gasification reactions.

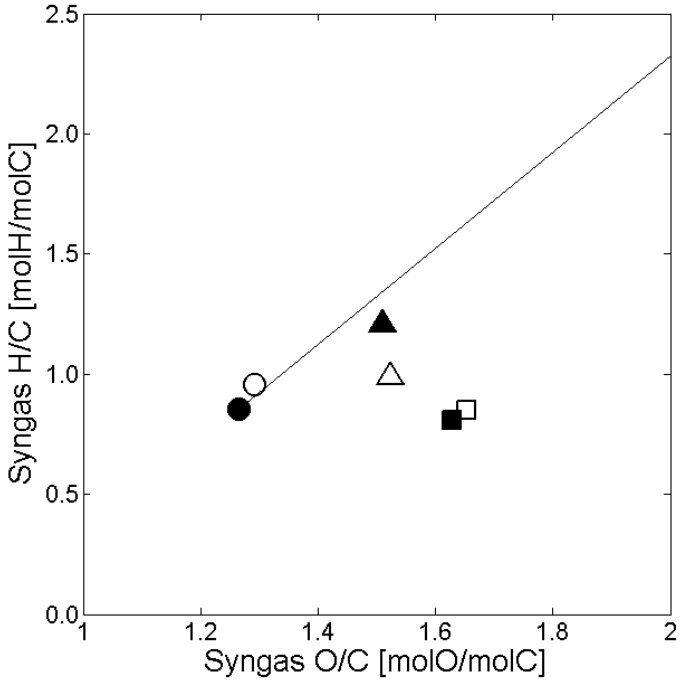

Figure 19: Molar H/C- and O/C-ratios of the produced syngas species. ● and ○: Low and high levels of fluidization with sand as the bed material, respectively; ■ and □: low and high levels of fluidization with ilmenite in the bed material, respectively; ▲ and Δ: CLR with 1.0% and 2.2% oxygen in the air reactor, respectively.

As stated above, both the employed measures (Sections 5.1 and 5.2) show potential for reducing significantly the tar yield. However, the performed measurements also raise questions as to how the yield of benzene can remain near constant throughout the measurements, as well as to how increasing the level of fluidization can lower the tar yield for sand but increase it when ilmenite is present in the bed. This suggests that there is an error in the measurement of benzene, and that additional, unquantified species affect the measured tar level.

5.3 SPA

The reproducibility of the SPA method was investigated in a series of eight measurements in the Chalmers DFB gasifier. Figure 20 shows the cumulative mass fractions, of known species and unknown groups, in all the measurements, compared to the relative standard deviations (%RSD). It is clear that while some species show a high %RSD, the majority of the mass fraction has a %RSD value that lies well within 10%. As shown in Paper 3, the RSD is noticeably high for the BTX compounds, due to incomplete adsorption. The %RSD was also high for all species that were detected at low concentrations, close to the detection limit of the analysis method. Moreover, some of the unknown groups, which comprise several species at low concentrations, show a high standard deviation. As discussed previously, the incomplete adsorption of the BTX species was confirmed by employing a new column, which also contained active carbon, in addition to the previously used amino phase. Thus, the

measurements shown in Papers 5 and 6 utilize the new column to ensure adequate quantification of the lighter tar species.

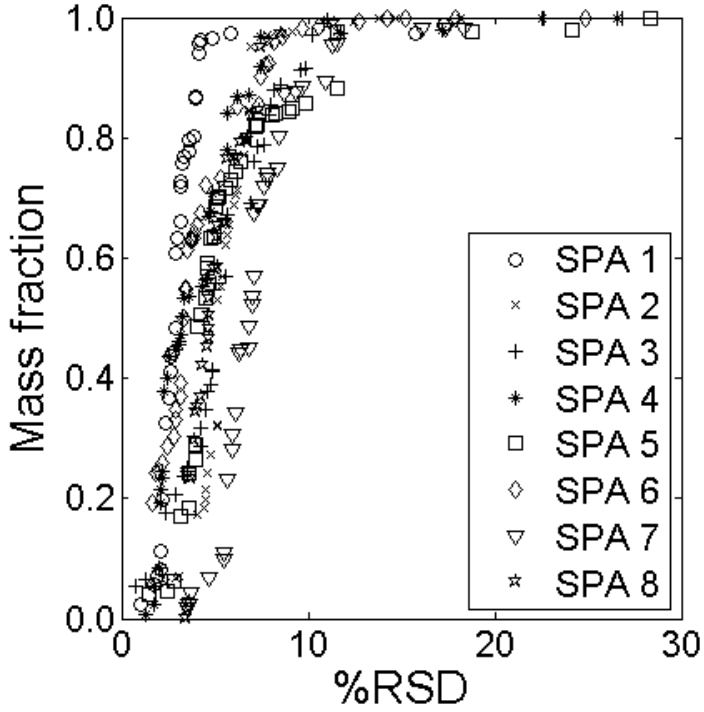

Figure 20: Cumulative mass fractions of known species and unknown groups in the tar exiting the Chalmers DFB gasifier as a function of %RSD for eight measurements with the SPA method.

Figure 21 shows more detailed profiles of the two measurements at the extreme ends, i.e., SPA 1 and SPA 7, as well as that of the intermediate measurement, SPA 2. Similar data were added from a GC calibration standard to depict a "best case" measurement. The %RSD of the GC varies slightly over time, although it is significantly lower than the %RSD obtained for all the collected samples. This indicates the potential for further improvements to the method. It is not clear whether the differences in repeatability between the three samples result from a fluctuating gasification process, incorrect sample collection, or an error in the analysis. However, the similarity of the curve shapes implies that the error affects to the same extent all of the groups in a sample. An error induced during the elution or analysis would almost certainly affect the volatile species differently than it would the heavier species. Therefore, the differences in repeatability between the measurements are most likely related to the gasifier or the sample collection.

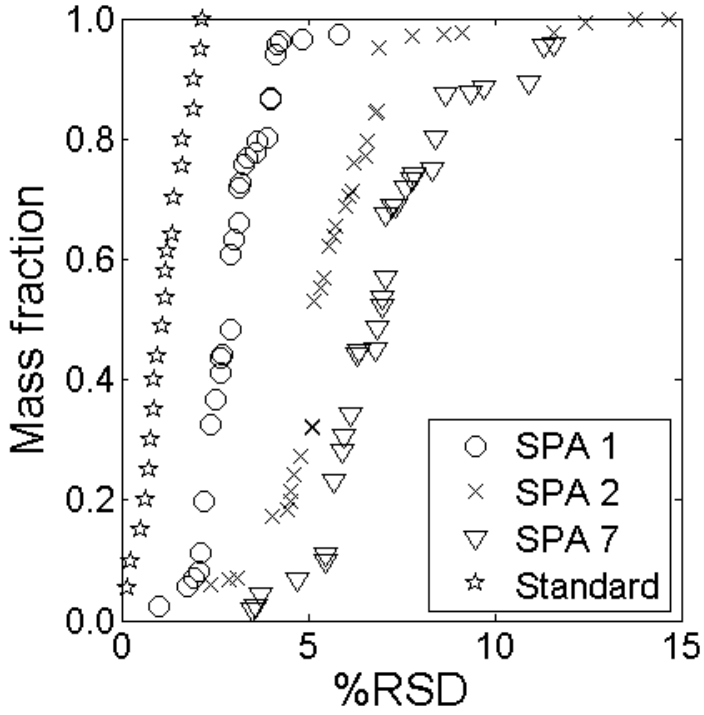

Figure 21: Cumulative mass fractions of known species and unknown groups in the tar exiting the Chalmers DFB gasifier as a function of %RSD for three measurements with the SPA method. Standard, GC calibration standard.

The GC analysis method was designed to allow the detection of species with boiling points within the boiling-point ranges of benzene to coronene. However, in all the measurements performed, only minor amounts of heavier tar components were detected, and coronene was not found in any sample (Figure 22). Initially, it was suspected that the heavier tars might have condensed on the filter or gas line. However, measurements performed on samples collected before the filter did not produce different results. Furthermore, from the time of their construction, the gasifier and sampling system have undergone more than 1000 h of operation at 350°C, without any signs of fouling or blockage in the equipment. Therefore, it was concluded that the obtained measurements relate to the heavy end of the tar spectrum produced in the Chalmers gasifier.

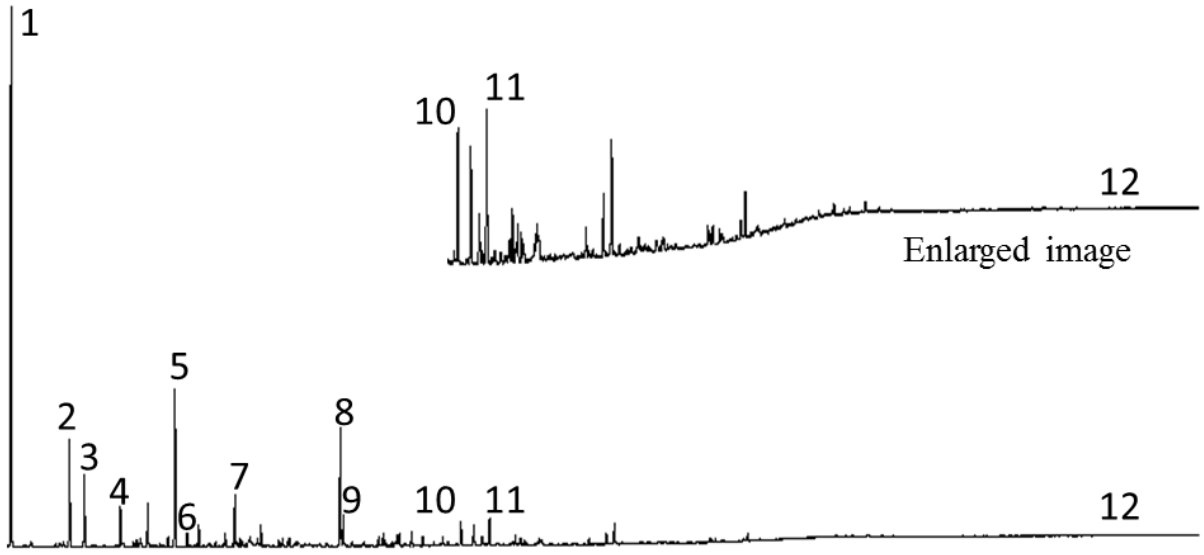

Figure 22: Segment of a chromatogram displaying the following peaks: 1, naphthalene; 2,2-methylnaphthalene; 3, 1-methylnaphthalene; 4, biphenyl; 5, acenaphthylene; 6, acenaphthene; 7, fluorene; 8, phenanthrene; 9, anthracene; 10, fluoranthene; 11, pyrene; and 12, coronene.

5.4 High-Temperature Reactor

Synthetic gas measurements were performed on a known gas mixture to determine the degree of conversion, as well as the levels of accuracy and soot formation as a function of temperature. The average values obtained from the synthetic gas measurements performed at 1700°C are presented in Table 3, together with the composition of the synthetic gas mixture. Sufficient conversion of large species was obtained, with only trace levels of CH_4 and C_2H_4 exiting the reactor system. Furthermore, the total volume of dry gas was increased by a factor of 1.82, as determined by the concentration of helium, due to the cracking of larger molecules and the WGSR.

The concentration of nitrogen is not affected to the same extent due to an exchange of gas between the measured gas and the volumes that were purged with nitrogen prior to the measurement. However, this exchange of gas is small at <1 vol% of the flow exiting the reactor. After the publication of Paper 4, the pack box (6) in Figure 12 was redesigned, resulting in significantly lower levels of gas exchange between the reactor and oven.

Table 3: Compositions of the inlet and outlet streams of gas during synthetic gas HTR experiments conducted at 1700°C.

Species	H_2	CO	CO_2	CH_4	C_2H_2	C_2H_4	C_3H_8	He	N_2
Feed gas [vol%]	25.2	39.52	8.94	11.9	0.496	4.99	0.994	4.97	2.99
Exiting gas [vol%]	54.31	29.13	11.45	0.05	N.D.	0.03	N.D.	2.73	2.30

N.D., not detected

The soot yields from the validation experiments, expressed as fractions of the supplied carbon [mass%], are presented in Figure 23. The amounts of soot collected after the HTR are shown as a function of the reactor temperature during operation at 1500°C, 1600°C, and 1700°C. There is a clear trend toward significant yields of soot at operating temperatures below 1700°C. The level of soot formation within the HTR is, most likely, much higher than the measured yields. Therefore, the difference between the measured points is more dependent upon the gasification of formed soot than the differences in soot formation. This emphasizes the need for rapid transport to the hot zone of the reactor, *via* the narrow tube shown in Figure 12, thereby limiting the attachment of soot to the walls in regions that are too cold to support soot gasification.

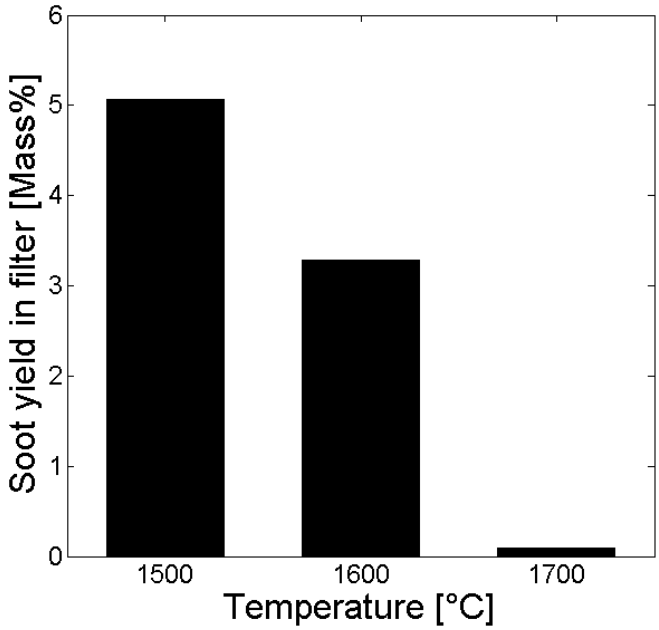

Figure 23: Yields of soot [mass%], for the validation experiments, collected in the filter as a function of temperature in the HTR at 1500°C, 1600°C, and 1700°C.

The elemental yields and estimated errors of the analysis for the validation experiments are reported in Paper 4 and are summarized as follows. The measured carbon yield in the reformed gas corresponds to 99.83% of the carbon in the synthetic gas, which is within the error of the employed analysis equipment. Furthermore, the amount of carbon recovered as soot in the DPF was 0.09% of the supplied carbon at 1700°C, which is in good agreement with the determined gas yield. The determined dry-gas yields of oxygen and hydrogen are both significantly >100% due to the WGSR. Consequently, it is not possible to determine their individual errors, in terms of yields, in the absence of an accurate steam measurement. However, as shown in Paper 4, the combined effect of these two errors can be determined by quantifying the oxygen addition. The determined error in oxygen addition was 2.8% of the oxygen supplied in the synthetic gas, indicating a significant level of added oxygen in the HTR. This could be caused by inward air leakages, the presence of pockets of air inside the reactor system or the outward leakage of hydrogen. To determine the actual cause, accurate measurements of the steam before and after the reactor are needed, which would allow

individual quantification of the levels of hydrogen and oxygen. However, the accuracy of the oxygen addition in Paper 4 is limited to that of the reactor system.

5.4.1 Applied Measurements

The HTR system was used in combination with the gas conditioning system (Figure 9) to perform measurements in the Chalmers DFB gasifier.

The average concentrations [vol%] of the species that exited the HTR are shown in Table 4, together with the concentrations of the species in the cold gas. The results show a very high degree of conversion of hydrocarbons that are heavier than methane, the level of which was close to the detection limit of the method. Furthermore, the level of tar exiting the HTR, as measured using the SPA method, was negligible compared to the background noise of the analysis.

Comparing the nitrogen concentrations in the two systems, it is evident an inward leakage of air occurred prior to the HTR. However, the use of two parallel measurement systems for the HTR gas and the cold gas enables quantification of the leaked air. Thus, the leak can be compensated for in the subsequent calculations. The nitrogen in the cold gas is supplied by the fuel feeding system and is compensated for in a similar way.

Table 4: Levels of components of the cold gas and HTR gas from measurements performed in the DFB gasifier.

Species	H_2	CO	CO_2	CH_4	C_2H_2	C_2H_4	C_2H_6	C_3H_6	He	N_2	H_2S
Cold gas [vol%]	32.21	19.57	29.55	8.31	0.11	2.51	0.43	0.25	1.07	5.37	0.61
HTR gas [vol%]	46.01	32.06	13.70	0.02	N.D.	N.D.	N.D.	N.D.	0.66	7.55	N.D.

N.D., not detected

The measured amounts of carbon, relative to the levels in the fuel feed, after the HTR and the gas conditioning system, are shown in Figure 24 for nine measured points. The difference in carbon yield between the two measurements reflects the amount of carbon present in the condensable species, as calculated using Eq. (3) and indicated by the double-arrow in Figure 24.

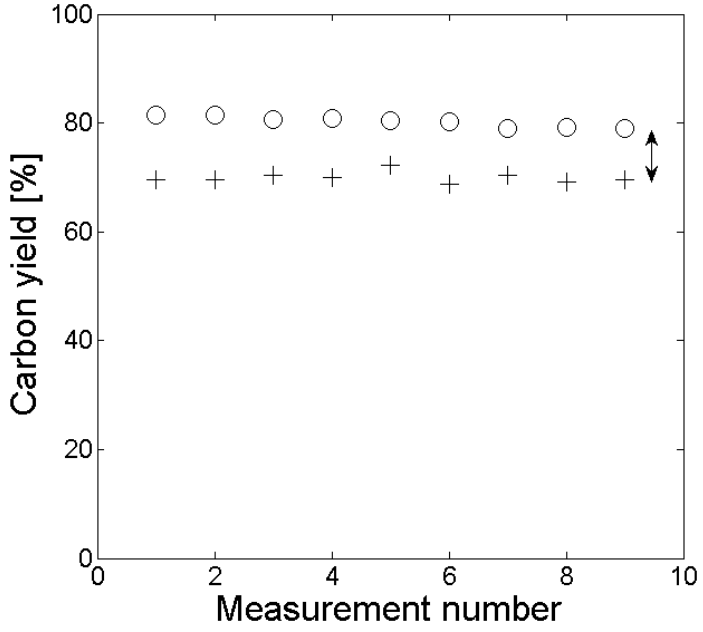

Figure 24: Relative carbon yields in the cold gas (+) and HTR gas (o).

The average concentration of CS, expressed as a function of the H/C-ratio is depicted in Figure 25 as a solid line that starts at the CH_{min} value, together with the H/C-ratio and concentration of tar measured by SPA. The graph also contains the CH_{min} value and concentration of the UCS, obtained by subtracting the SPA tar level from the average level of CS. The dotted lines represent the standard deviation of the analysis. The H/C- and O/C-ratios for the total condensable species increase from the CH_{min} value and zero, respectively, owing to the addition of water (Figure 26), according to Eq. (4). As shown in Figure 25, the concentration of UCS, at CH_{min}, is more than twice that of the measured tar, using the SPA method. This shows the importance of fulfilling the mass balance of the system, as roughly 6% of the carbon content of the provided fuel is found as UCS. In line with the tar measurement shown in Figure 22, only minor amounts of heavy tar species were detected in the performed SPA measurements. This indicates that the H/C- and O/C-ratios of the UCS are significantly higher than the CH_{min} value and zero, respectively, reflecting the presence of species that are either lighter than benzene or highly oxygenated. It should be noted that these tar measurements were not performed using the improved SPA method and, therefore, the UCS will include a significant amount of BTX species.

Measurements of the incoming steam and the condensate in the raw gas would enable determinations of the H/C-ratio and corresponding O/C-ratio of the CS. However, the amount of water needed to increase the H/C-ratio from the CH_{min} value (0.83) to 1.5 is <3 mass% of all the incoming steam. Therefore, the mass balance of water in the gasifier system needs to be determined with high accuracy to yield useful information concerning the H and O contents of the CS. Nevertheless, as the condensable compounds contain low amounts of water, their effects on the raw gas concentration of the steam is negligible. Consequently, the concentration of steam can be calculated using data on the flow and composition of the cold gas, the condensable compounds described by CH_{min}, and the steam input to the gasifier. An

average tar molecule is chosen to determine the volumetric flow of condensable compounds, in this case, benzene. Furthermore, if the steam input is not known, it can be derived by comparing the cold gas with the wet gas exiting the HTR.

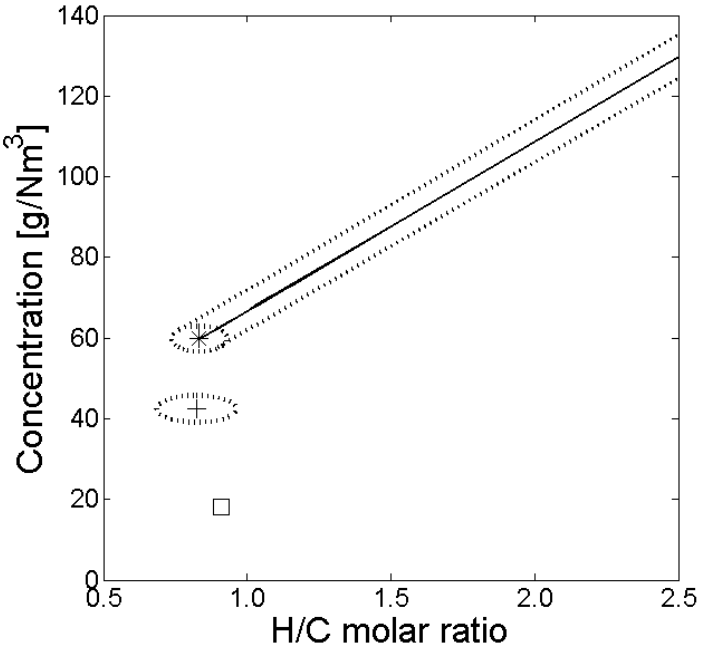

Figure 25: Concentrations, as a function of the H/C-ratio of CS (∗), of UCS (+) at the CH_{min} value, and for the SPA-analyzed tar (□).

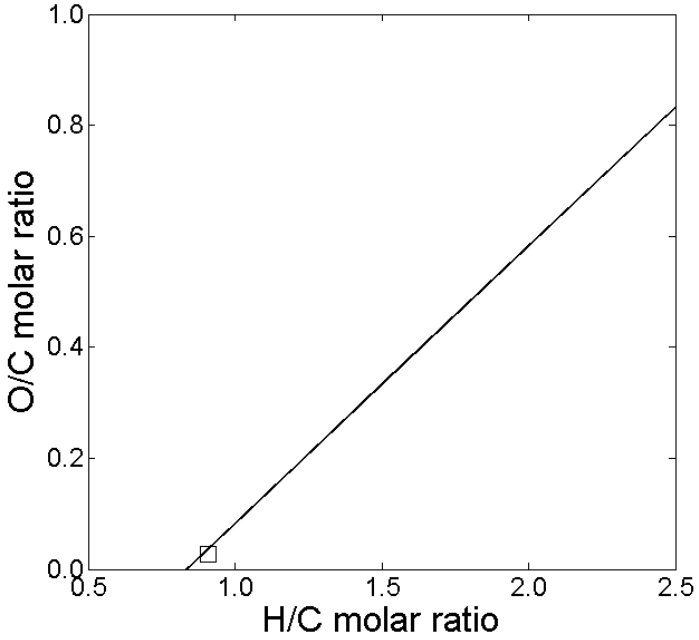

Figure 26: O/C-ratio as a function of the H/C-ratio for the CS and SPA-analyzed tar (□).

The ability to determine precisely the H/C- and O/C-ratios of the condensable compounds is of great value, as it generates information concerning the true concentration and, possibly, the size range and boiling point, of the UCS. However, the energy content can be determined without this information, provided that the carbon flows and CH_{min} are known. The calculated cold gas, raw gas, and theoretical raw gas efficiencies were 61.4%, 73.5%, and 81.8%, respectively, and the raw gas LHV was 7.11 MJ/Nm^3, according to Eqs. (7−9). Consequently, 12.1% of the energy in the fuel was found in the CS. This corresponds closely to the results from previous studies[45], which report values that range from around 20% for pyrolysis to 10%−15% for DFB gasification with sand. Furthermore, the carbon yield of the CS, presented in Figure 24, corresponds to approximately 10% of the carbon content of the fuel or 5 mass% of the dry-fuel feed. This agrees well with presented data for fluidized bed gasifiers[2].

If a gas conditioning system is not available, the raw gas LHV can be estimated using only the data obtained from the HTR system. In Figure 27, the calculated equivalent LHVs of the wet raw gas, as well as the LHV of the wet HTR gas, are shown relative to the measured LHV for the wet raw gas. The measured values of the raw and HTR gas LHVs fall within the interval of the maximum hydrogen and methane yields. Furthermore, the methane-equivalent LHV differs from the measured value by 1.3%. The other equivalent species, from ethane to acetylene, overestimate the heating value for the produced gas.

As previously mentioned, different process types will have different optimal equivalent species. For example, high-temperature gasification for syngas production can be best described using an equivalent syngas mixture with composition that lies somewhere between the maximum theoretical yields of H_2 and CO. Similarly, the DFB gasification measurements performed in the present study reveal good agreement with the methane-equivalent heating value.

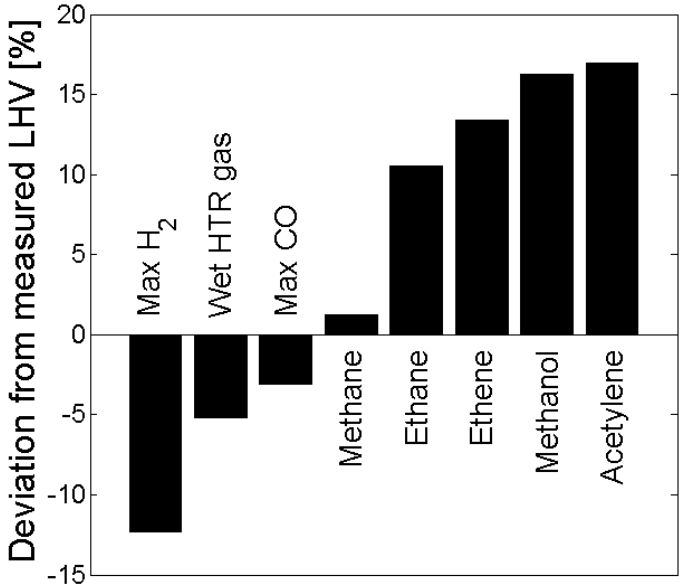

Figure 27: Deviations in the calculated LHVs of the wet raw gas from the measured LHVs of the wet raw gas for HTR gas and equivalent gases and gas mixtures.

The improved SPA method, together with the measurements developed using the HTR, allow new levels of accuracy and quantifiable segments of the raw gas spectrum. This additional information meets the previously stated demands on the measurements and helps to explain behaviors similar to those observed in the initial part of this section. Nevertheless, additional experiments are needed to identify trends for the newly created groups and phenomena as functions of varying process parameters.

5.5 Parameter Study for DFB Gasification

The experimental results obtained during the parameter study covered by Paper 5 are presented below to show the individual effects of the average raw gas temperature, steam-to-fuel ratio, and residence time observed when silica sand was used as the bed material in the gasifier. The employed process parameters are depicted in Table 2.

The collected data for all experimental points are summarized in Figures 28–30. The first set of plots (Fig. 28, A and B) describes the effects of the average gas temperature, while the remaining two sets (Figs. 29 and 30) describe the effects of fluidization (the steam-to-fuel ratio) and residence time (fluidization at constant steam-to-fuel ratio), respectively. For all the sets of plots, panel (A) depicts the measured yields of cold gas species (in mol/$kg_{daf\ fuel}$), and panel (B) depicts the carbon mass balance of the gasifier system together with the oxygen transport (expressed as the stoichiometric air-to-fuel ratio; AFR). The carbon balance consists of the carbon yields (relative to the fuel feed) of the cold gas, char, and CS, together with the yields of SPA and UCS. As previously stated, all the SPA measurements were performed using two types of columns, to allow quantification of the BTX-species; consequently, the presented values for SPA tar include benzene. Unfortunately, for measurement T758, leakage occurred in the SPA sampling equipment, which resulted in an insufficient volume of raw gas being sampled for the carbon-containing columns. This leak was compensated for by comparing the collected amount of naphthalene to that collected in the columns without carbon, to obtain a more accurate estimation of the BTX-species. Naphthalene was chosen because it is present at high levels and is readily captured by both column types. The corrected yields (represented by '-') of the SPA-detectable tar and UCS are shown together with the measured yields in Figure 28B.

5.5.1 Temperature

The measured molar yields of the various cold gas components, at three different raw gas temperatures, are displayed in Figure 28A. The performed measurements show clear trends towards increasing levels of all gas species up to C_2H_4 and decreasing levels of C_2H_6 and C_3H_6, as the temperature increases. Similarly, in Figure 28B, the collected data-points show clear trends towards increasing cold gas yields and decreasing yields of char and CS as the raw gas temperature increases. These results are as expected and are in line with previous results obtained for biomass gasification.

The decrease in CS is mainly due to a decrease in the yield of UCS, which in turn seems to produce cold gas and CS that can be measured using the SPA method. As a result, the yield of

SPA tar increases with increasing temperature. Indeed, for measurement T774, the yield of carbon in the UCS is close to zero, and the carbon balance can be resolved using only the SPA and cold gas measurements. Presumably, from the point of high temperature, the SPA tar yield would decrease if the temperature was increased further. However, this might also cause the yield of UCS to increase owing to the polymerization of heavier tar species. These results help to explain why the mass balance is generally more difficult to resolve at lower temperatures[44], as well as why the measureable tar fraction can increase as a result of an increase in temperature[28, 35].

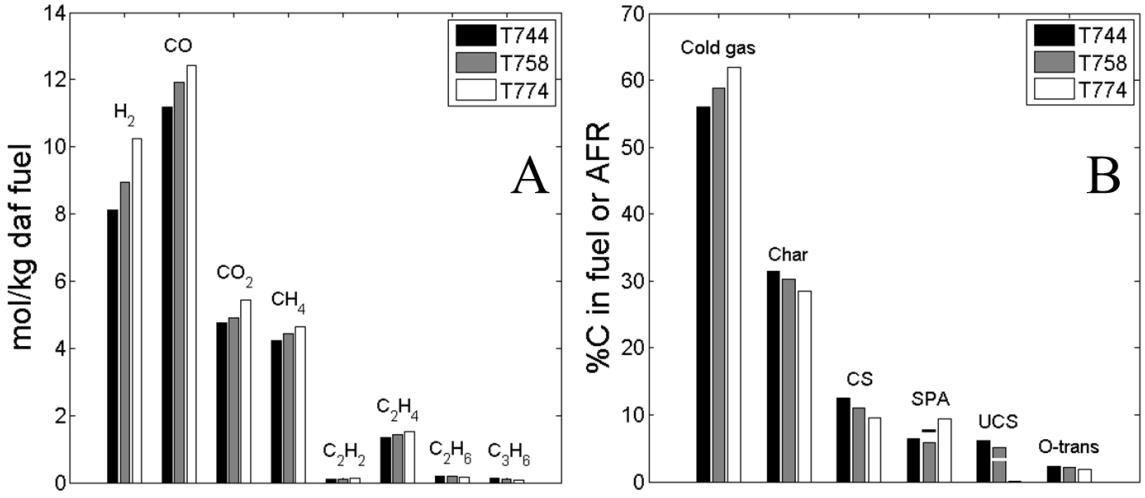

Figure 28: (A) Molar yields (mol/kg$_{daf\ fuel}$) of the cold gas species as a function of the average raw gas temperature. (B) Fractions of the introduced carbon in the cold gas, char, CS, SPA-tar, and UCS, as well as the oxygen transport, shown as the AFR ('-' denotes corrected values for SPA-detectable tar and UCS).

5.5.2 Steam-to-fuel Ratio

In similarity to the above results, Figure 29 depicts the measured and calculated yields of the relevant streams at three different levels of fluidization. The cold gas measurements (Fig. 29A) show an enhanced effect of the WGSR as the level of fluidization is increased, possibly due to the increased steam-to-fuel ratio or increased gas-solid contact. Despite this increased reactivity, the cold gas efficiency decreases slightly as the level of fluidization is initially increased (62.4%, 59.9%, and 60.1%, respectively). This is explained by the carbon balance in Figure 29B, which shows a decrease in char conversion as the level of fluidization is increased. At higher levels of fluidization, the char particles are more readily transported by the bed material, resulting in shorter residence times and a lower level of conversion[43, 58].

A noteworthy result is that while the yield of SPA-detectable tar decreases with increased fluidization (similar to the sand cases in Figures 17 and 18), the total yield of condensable species initially increases due to an increase in the yield of UCS. Consequently, the decrease in SPA-detectable tar is not attributable to it being consumed by various reactions that involve steam, but rather to the fact that it is not being formed through the reformation of UCS. This decrease in UCS reforming is in good agreement with the observation that the residence time

of the gas is decreased at higher levels of fluidization. At even higher levels of fluidization (S190), the total yield of CS is decreased slightly, most likely due to an increase in either the degree of gas-solid contact or the temperature. However, the yield of UCS is still higher than that obtained at low levels of fluidization. In summary, for the studied cases, the main effect of increasing the level of fluidization (to obtain higher steam-to-fuel ratios) is shorter residence times in the freeboard and bed. This results in decreased char and UCS conversion, the latter of which can be misinterpreted as the reforming of SPA-detectable tar.

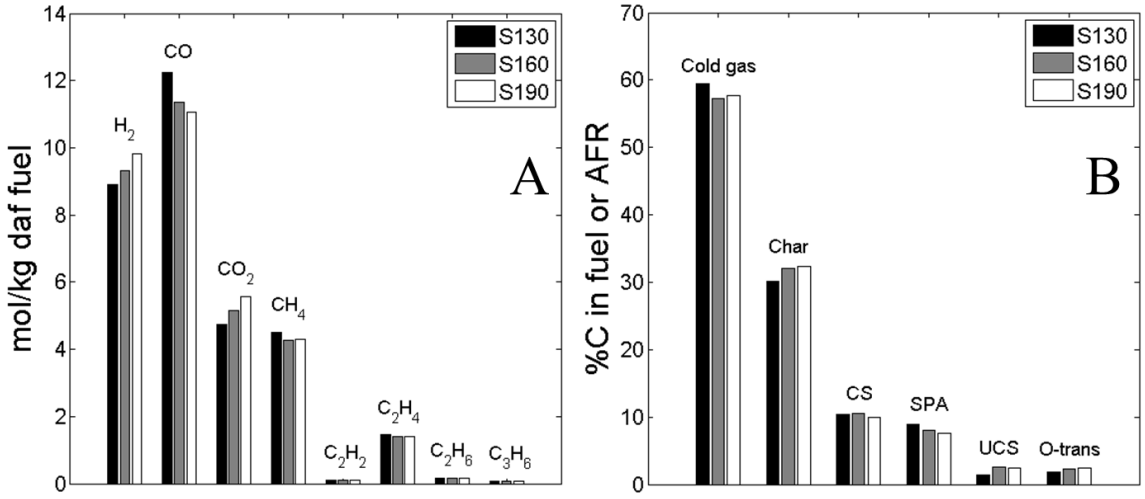

Figure 29: (A) Molar yields (mol/kg$_{daf\ fuel}$) of the cold gas species as a function of the fluidization in the gasifier. (B) Fractions of the introduced carbon in the cold gas, char, CS, SPA-tar, and UCS, as well as the oxygen transport, shown as the AFR.

5.5.3 Residence Time

The steam and fuel feeds were changed simultaneously to obtain three points with similar steam-to-fuel ratios but with different residence times and degrees of gas-solid contact (Fig. 30). The cold gas measurements (Fig. 30A) resemble those obtained from the experiments with increased fluidization, in terms of the levels of CO, CO_2, and CH_4. Nevertheless, despite an initial increase in the WGSR as the flows of steam and fuel increased, the hydrogen yield decreases due to the significant drop in char conversion. For even shorter residence times, the extent of the WGSR decreases slightly. This implies that the increased extent of the WGSR observed for the high fluidization point in Figure 29 is due to the increased steam-to-fuel ratio, as the gas-solid contact should be similar. In line with the carbon balance in Figure 29, the char conversion decreases with increased steam flows.

The total yield of CS at the point with the lowest flow in Figure 30B resembles that for the high temperature in Figure 28, in the sense that all the CS are found as SPA-measureable tar. This suggests that these points produce the most evolved tar profiles of this study, obtainable at sufficient temperatures and residence times. The behaviors of the CS throughout Figure 30 show clear trends that describe increasing yields for both the total and unidentified CS, while the yields of SPA-measured species decrease. In line with the results obtained when

increasing the fluidization, this suggests that the CS are not as evolved due to the decreased residence time.

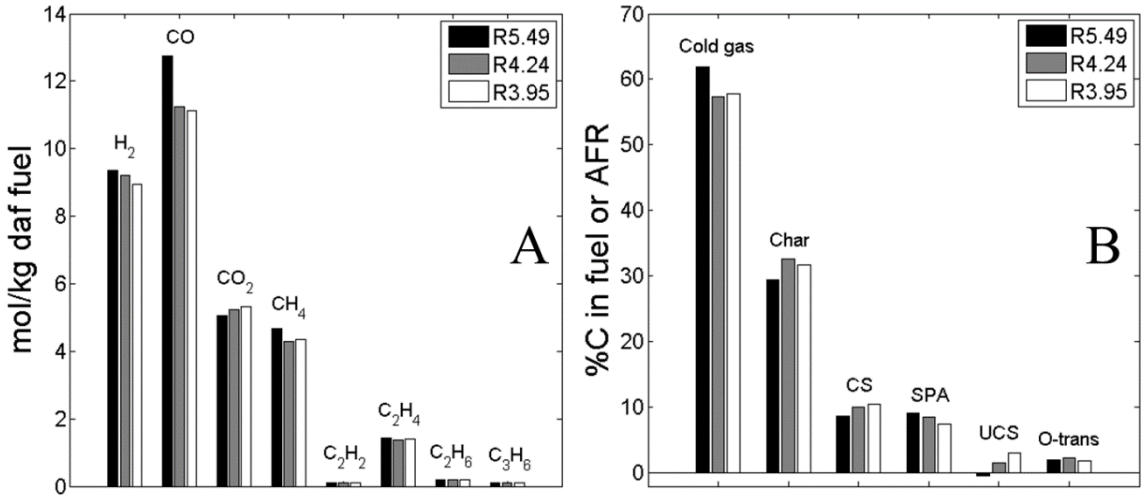

Figure 30: (A) Molar yields (mol/kg$_{daf\ fuel}$) of the cold gas species as a function of residence time. (B) Fractions of the introduced carbon in the cold gas, char, CS, SPA-tar, and UCS, as well as the oxygen transport, shown as the AFR. The UCS yield of R5.49 is considered to be zero; the obtained negative value relates to the uncertainty of the measurement.

5.5.4 Effects on Condensable Species

As described in the previous sections, the UCS are strongly related to the SPA-measureable species. This underlines the importance of describing their behaviors in such a way as to understand and predict the behavior of the measureable tar. The obtained yields of UCS and SPA-measureable tar from the silica-sand measurements are shown as a function of temperature and residence time in Figure 31. Here, all the points are represented as pie charts, relative to the point at low temperature that produces the highest yield of CS. For example, comparing the data-points for the high and low temperatures, the total amount of CS is reduced by roughly 25% (white segment), all the UCS (gray segment) are converted, and the SPA-detectable tar yield (black segment) is increased by ~50% with respect to the reference T744. Furthermore, the fact that all the UCS are converted at high temperature indicates that the implementation of the SPA method in Papers 5 and 6 successfully quantifies benzene, since undetected benzene would appear as UCS. As mentioned previously, the question as to whether the average gas temperature is representative of the conditions in the freeboard remains to be resolved. Nonetheless, it is suitable for describing the differences between the performed experiments.

As shown in Figure 31, the UCS yield exhibits negative trends for both increased temperature and residence times. Furthermore, the opposite trends can be seen for the SPA-detectable species. Overall, the yield of UCS ranges from near-zero values, at high temperatures and long residence times, to yields that are comparable to those of the SPA-detectable species at low temperature. The observed response of the UCS to increased severity in the gasifier is not

consistent with that expected from large poly-aromatic species[2]. This, in line with the findings of van Paasen *et al.*[48], indicates that the UCS are comprised mainly of primary and secondary tar species according to the classification constructed by Evans and Milne[2]. As a result, the UCS can be considered as being oxygenated, with a composition similar to that of the fuel, or as reactive intermediate species.

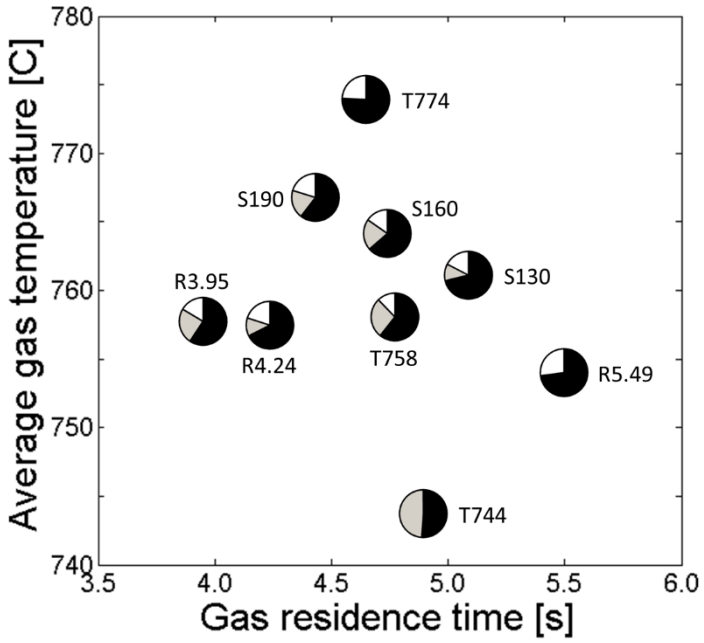

Figure 31: Normalized yields (relative to the total CS yield of T744) of UCS (gray segments) and SPA species (black segments) as a function of temperature and residence time.

Based on the obtained results, the observed relationship between CS, UCS, and SPA tar is depicted in Figure 32 as a function of increasing severity. At low levels of severity, corresponding to low-temperature pyrolysis, UCS is assumed to be the dominating species. As the severity is increased, the UCS is gradually converted into SPA tar and cold gas until the CS is comprised exclusively of SPA tar. The performed experiments (indicated in the figure) include this point, although, as previously stated, it is possible that a different type of UCS forms as the level of severity is further increased.

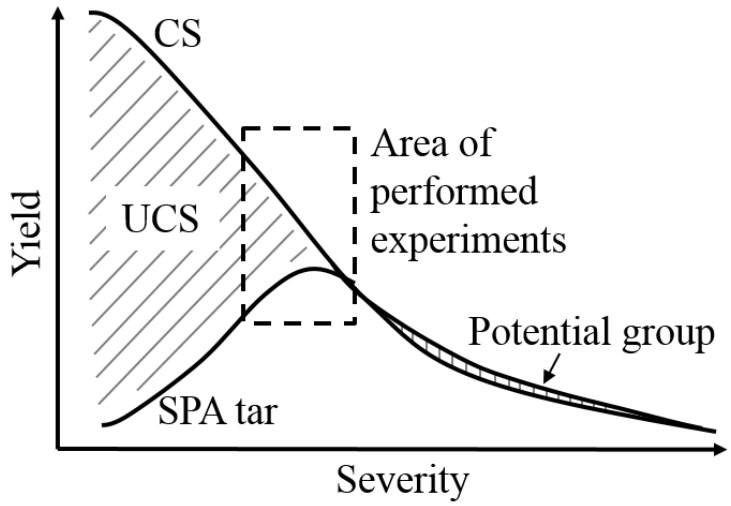

Figure 32: Evolution of the CS as a function of the level of severity.

5.6 Reaction Scheme of Condensable Species

During initial attempts to construct a general set of reaction expressions in Paper 6, it was noted that the experimental points collected through varying the residence time (Table 2) did not comply with the remaining data-points. This is also implied in Figure 31, where point R4.24 stands out from the general trend. Therefore, these data-points were excluded from the numeric solver, and were subsequently used for comparison with the obtained model during the later stages of this work. The two exponents x and y in Eq. (11) were, as described above, determined by solving analytically the individual reaction expressions for UCS and phenol. The resulting values for x and y were approximately 2 and 1, respectively, and they were used to describe the reactivities of all the species, with the exception of primary F, for which an x-value of 2.3 was obtained. Presumably, the actual values for x and y may vary between different species, but it is unlikely that such variations would be large enough to alter the findings of this study. It was similarly concluded that a reaction order of one should be used for all the CS.

The evolution of the various groups of CS, as described by the obtained reaction parameters, is shown in Figures 33–38 for the three cases that describe the situations with high (792˚C), medium (774˚C), and low (758˚C) temperatures. The lines indicate the modeled trends, while the data-points represent the measured values. In all the figures, the triangles correspond to the dashed lines and the circles correspond to the solid lines. As previously mentioned, it is assumed that all the CS are present as primary UCS at the starting point, and that all the other species are formed through its decomposition. Overall, the derived parameters provide a reasonably good fit to the provided data, which means that the derived scheme ably depicts the general trends of the measurements. Similar curves for the measurements obtained at different levels of fluidization are comparable to those obtained at the medium temperature. The main effects of altering the level of fluidization are alterations of the residence time and the concentrations of the tar species, with the latter being due to dilution by the steam. The derived relative rate coefficients, which result in the best fit, are summarized in Appendix A of Paper 6.

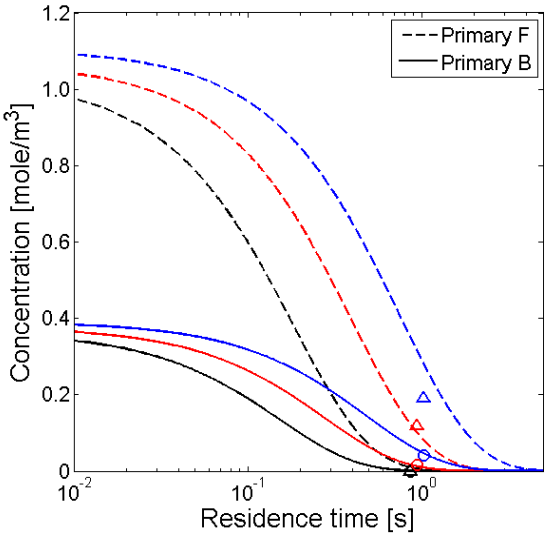

Figure 33: Evolution profiles of the primary UCS at high, medium, and low temperatures, shown as black, red, and blue lines, respectively.

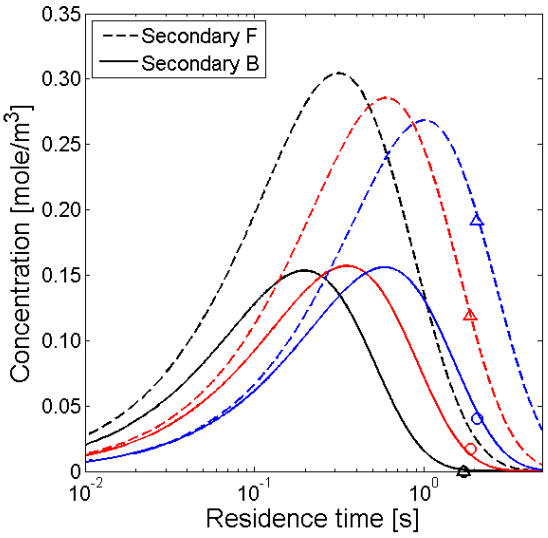

Figure 34: Evolution profiles of the secondary UCS at high, medium, and low temperatures, shown as black, red, and blue lines, respectively.

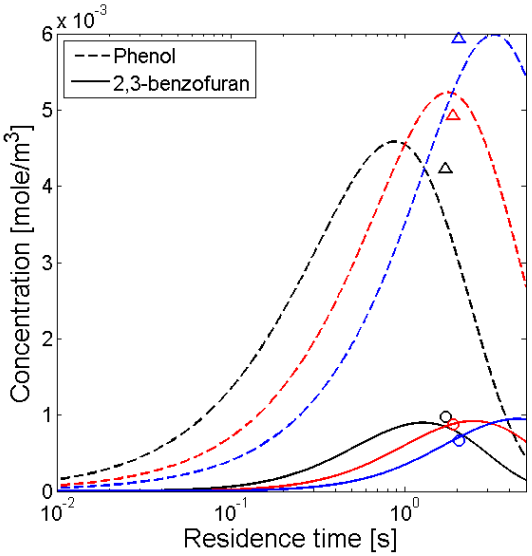

Figure 35: Evolution profiles of phenol and 2,3-benzofuran at high, medium, and low temperatures, shown as black, red, and blue lines, respectively.

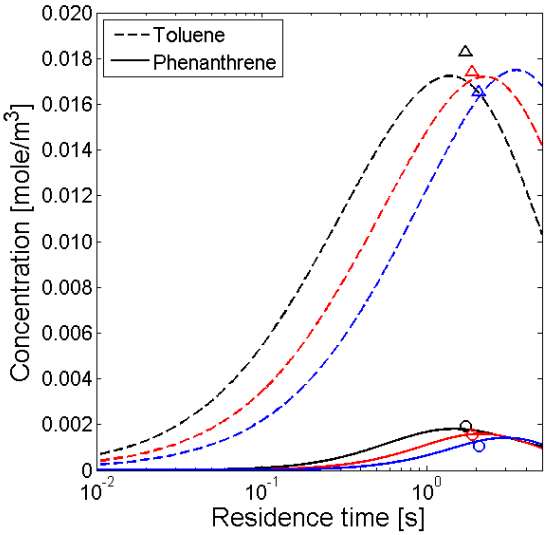

Figure 36: Evolution profiles of toluene and phenanthrene at high, medium, and low temperatures, shown as black, red, and blue lines, respectively.

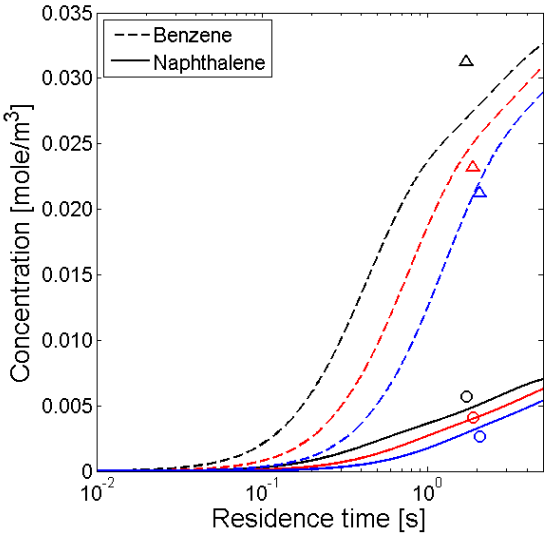

Figure 37: Evolution profiles of benzene and naphthalene at high, medium, and low temperatures, shown as black, red, and blue lines, respectively.

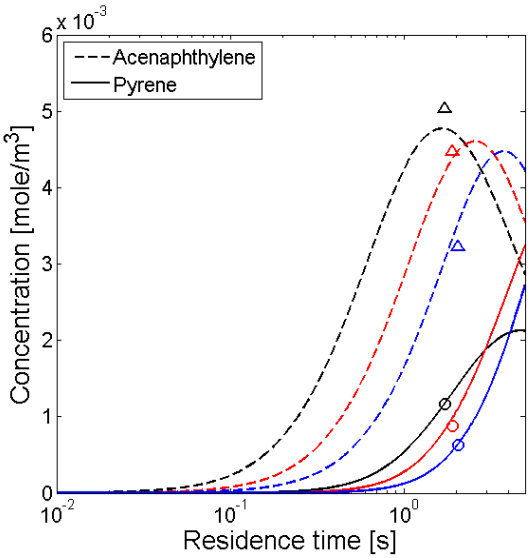

Figure 38: Evolution profiles of acenaphthylene and pyrene at high, medium, and low temperatures, shown as black, red, and blue lines, respectively.

The derived reaction scheme and distribution factors are presented in Figure 39 and Table 5, respectively. In Figure 39, all the reaction routes that involve UCS and UCS′ are assigned two distribution factors, with the odd numbers referring to F and the even numbers referring to B for all the routes. The thickness of the lines that denote the different routes indicate how much carbon was transported *via* a specific route during the first 5 seconds of the reactions. The dashed lines all transported 5-times less mass than a solid line of equal thickness. It should be noted that while the thick lines represent significant routes of mass transfer, the thin and dashed lines are less certain and arise from the employed solver and reaction scheme. As all the routes represent global reaction mechanisms, higher levels of resolution are needed to describe properly the transport of lower amounts of mass between the various groups. Nevertheless, upon investigation of the less significant routes, it was found that reactions regarded as being unlikely, such as the formation of furan from phenol, agreed well with the findings of earlier studies[2, 22, 59]. The green lines in Figure 39 indicate routes of mass transfer that proceed directly from UCS′ to much more mature tar species, owing to the previously mentioned polymerization of species, such as cyclopentadiene. In addition to the mass transfer that occurs between the different tar species, the reactions yield various amounts of cold gas species, although these routes are not included in the figure. Interestingly, it was not possible to transport sufficient mass through the system without employing reaction routes 13–20. This implies that the contribution of UCS′, either as a direct reaction or as part of the polymerization reactions, is of great importance for both the creation and maturation of the SPA-tar. However, as shown in Table 5, the current model does not differentiate between F and B as long as enough mass is transported to the heavier species.

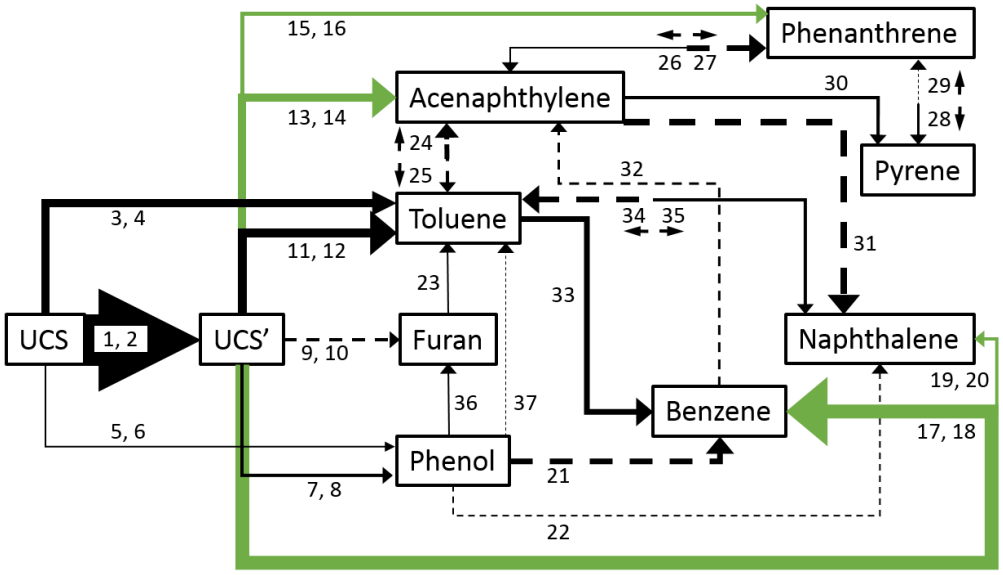

Figure 39: Proposed reaction scheme with numbers denoting relevant distribution factors and the line thickness indicating the significance of the path.

Table 5: Derived carbon distribution factors (according to Figure 39).

Route	1	2	3	4	5	6	7	8	9	10	11
	0.50	0.90	0	0.051	0.017	0	0.066	0	0.0093	0.0016	0.15
Route	12	13	14	15	16	17	18	19	20	21	22
	0.0021	0.15	0	0.075	0	0	0.10	0	0.022	0.33	0.11
Route	23	24	25	26	27	28	29	30	31	32	33
	0.84	0.11	0.11	0.43	0.17	0.57	0.28	0.53	0.19	0.22	0.58
Route	34	35	36	37							
	0.81	0.31	0.50	0.059							

The carbon distribution factors (summarized in Table 5) were assumed to be constant, regardless of the reaction type, temperature, reactant concentration or other process parameters. Allowing these constants to vary as a function of temperature and relevant concentrations would make the model more realistic and, presumably, more flexible. However, for the performed study, the impact of constant distribution coefficients is assumed to be low, given that the different cases considered are somewhat similar.

The proposed reaction scheme and model provide a satisfactory description of the observed trends during the maturation of biomass-derived tar. Furthermore, while a wider range of experimental points would have been desirable, the current data are sufficient to support the proposed reaction scheme and to show how SPA-tar can be formed from measureable (albeit unknown) CS. These results are in good agreement with those of Cypres[22], who showed that the formation of aromatic tar during coal pyrolysis encompassed the formation and dehydrogenation of cyclo-olefins, as well as the decomposition of phenol. This raises the possibility of reducing the total yield of CS while minimizing the production of the more stable species, such as benzene. Potential ways of accomplishing this are presumably best

implemented as primary measures and include converting the various UCS into gas before they can form SPA tar. Thus, complications related to high tar levels could be avoided at least in part at an early stage. This would probably be beneficial, as compared to implementing secondary measures to combat SPA tar, which is considerably more stable.

The derived model was applied to the measurements obtained when varying the residence times, to investigate the observed deviations. The predicted evolutionary profiles for the primary and secondary UCS are shown in Figures 40 and 41, respectively, together with the measured values. While the general trend of the modeled data reflects that of the measurements, the predicted behavior greatly underestimates the conversion of UCS. This, combined with additional shortcomings associated with the expressions for the remaining reactions, affects all the remaining species in the raw gas. The observed model deviations from the measured data result in part from incorrectly determined residence times and temperatures. However, additional factors, presumably related to aging of the bed material and gas-particle contacts in the freeboard, are needed to elucidate fully the changes in the reactivity of the CS[54, 55]. Consequently, the proposed expressions for reactivity should include the impacts of catalytic species, such as the concentration of ash components or a factor representing the catalytic surfaces in the freeboard. Interestingly, the experiments in which residence time was varied were the last to be performed in this study, which supports the notion that the observed change in reactivity relates to aging of the bed material. From the wider perspective, it should be noted that if these effects are not accounted for, rate expressions will only be applicable to the type of system for which they were derived, provided that the system does not exhibit significant variability in the levels of catalytic species.

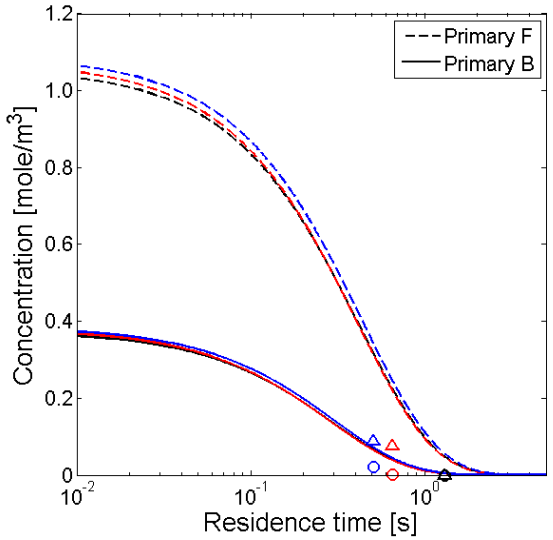

Figure 40: Evolution profiles of the primary UCS at long, medium, and short residence times, shown as black, red, and blue lines, respectively.

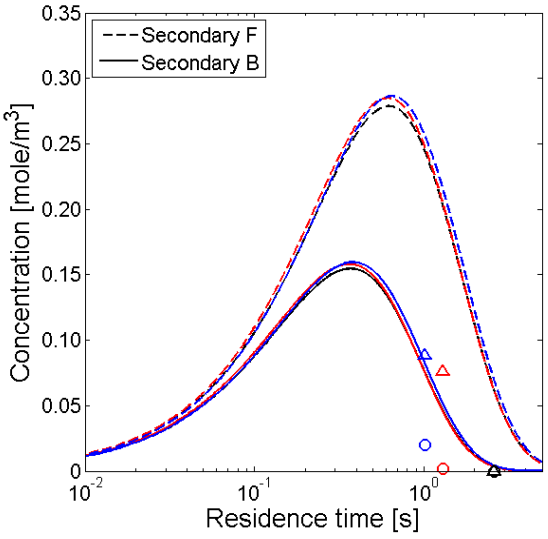

Figure 41: Evolution profiles of the secondary UCS at long, medium, and short residence times, shown as black, red, and blue lines, respectively.

The performed parameter study and subsequent modeling shows clearly the importance of UCS for the evolution of SPA-tar. This explains to some extent the behavior of the tar in the studies of the primary and secondary measures, as neither UCS nor benzene were represented

appropriately in the measurements. Similar to the measurements described in the first part of this section, these results can be used to indicate areas where the performed measurements can be improved. These include improved measurements within the gasifier to obtain profiles for the gas temperature and mixing, providing accurate data for determining the representative average gas temperatures and residence times. In addition, the raw gas measurements could be complemented by on-line measurements of soot and alkali, as well as by extended measurements of the CS to identify the major UCS components.

6 - Conclusions

The effects of catalytic bed materials on tar evolution were compared by implementing ilmenite ore in the Chalmers DFB gasifier and manganese ore in a CLR. Both approaches resulted in significant decreases, around 50% under optimal conditions, in the levels of tar. The changes in tar composition in the CLR followed the expected trends of tar maturation, resulting in higher levels of naphthalene and larger aromatic species. The changes in tar composition from the gasifier measurements differed significantly from those seen in the CLR. At low fluidization, the yields of all tar groups were decreased, whereas at higher levels of fluidization, the yields of both phenols and heavy species were least affected. From these measurements, it is evident that the manner of catalyst implementation potently influences its performance, and that a fulfilled mass balance is necessary to obtain a clear understanding of the raw gas behavior.

Comparing the gas compositions, in terms of the syngas components of CO, CO_2, and H_2, of the CLR and gasifier measurements, it is clear that oxygen transport is higher in the gasifier. This is due not only to different bed materials being used, but also because the bed material flow is determined by the heat demand of the gasifier and, as a result, it cannot be manipulated to minimize the oxygen transport. The heat demand of the CLR is much lower than that of the gasifier, resulting in a much higher potential for optimization of oxygen transport.

Two different methods of analysis were investigated for tar analysis and the elemental quantification of the raw gas to meet the required levels of measurement accuracy. The SPA method for measurement of tar species was evaluated with respect to detection limits and reproducibility. A majority of the mass of the collected samples was quantified with an RSD well within 10%. However, the absorption of lighter species, which ranged from benzene to xylene, was insufficient using the employed column. Since the publication of Paper 3, the method used for the elution of collected samples has been revised to entail fewer steps and chemicals. Furthermore, new sample extraction columns, which contain an additional bed of active carbon, are being used to quantify, with accuracy, the lighter tar species.

The HTR, which was developed for total elemental quantification of the raw gas, was evaluated in validation experiments. The determined values for carbon yield and soot formation were within the margin of error of the analysis. The measured error for oxygen addition was higher than the error of analysis, corresponding to 2.8% of the oxygen provided

in the dry synthetic gas mixture. The HTR was rebuilt after the publication of Paper 4, and there are currently no signs of any significant effects of internal gas exchange.

Online measurements using the Chalmers DFB gasifier enabled indirect determinations of the oxygen transport, the total carbon conversion in the gasifier, and the amount of condensable carbon, using mass balance calculations. The performed measurements were used to determine the lowest possible H/C-ratio, CH_{min}, of the CS. This was combined with the average oxygen-based heating value to calculate the energy content of the CS. Furthermore, using CH_{min} to represent the CS induces only a small error in the water balance of the system. This allows calculation of the steam concentration and the corresponding LHV of the raw gas. The methane-equivalent heating value, determined using only data from the HTR, was within 1.3% of the measured LHV in Paper 4.

The parameter study performed in Paper 5 shows a clear correlation between SPA-tar and UCS, whereby the conversion of UCS generates SPA tar. This, together with the behavior of the UCS at increased levels of severity, implies that this group consists mainly of oxygenated primary and secondary tar species, as well as reactive intermediate species. The obtained results help to explain the occasionally strange behavior of SPA-tar, and demonstrate the importance of quantifying all segments of the raw gas spectrum.

The reaction scheme derived in Paper 6 requires a significant contribution from the various groups of UCS (which generate SPA-tar directly) to produce satisfactory trends for the SPA-tar. This implies that the primary conversion of CS is crucial for describing the formation of measureable tar, and that measures that are implemented to reduce the tar yield should be focused on maximizing the gas yield from this conversion.

The derived rate expressions underestimate the reaction rate of the experimental data-points collected during the final day of the measurement campaign. This indicates that additional factors, such as bed material aging, gas-particle contacts, and mixing in the freeboard, can influence the reactivities of the CS. Consequently, current knowledge of the key parameters related to gasification is inadequate for describing accurately the behaviors of the CS. Provided that these factors are insignificant or remain constant, a functioning model can be constructed that does not take them into consideration. Nevertheless, such a model would only be applicable to near-identical systems, which motivates further studies of the behaviors and catalytic effects of ash components, and specifically of alkali compounds.

7 - Future Work

The tools and methods developed during this work offer the possibility of measuring accurately the entire raw gas spectrum. At present, there are several opportunities for further studies, in terms of improving both the measurement and the analysis of the results.

- The findings of Papers 5 and 6 indicate that additional information is required to describe the behavior of the gasifier, such as measurements of the gaseous alkali concentration, the level of gas-particle contact, and the soot yield. Furthermore, obtaining detailed profiles of the temperature and the mixing within the gasifier would improve the accuracies of the determined values for the gas residence time and the representative temperature.

- The inclusion of the suggested measurements in the model, together with a wider set of measurement data and a clearly defined starting point for pyrolysis, would give a better fit with the data. However, additional improvements, such as allowing the distribution coefficients to vary and the inclusion of cold gas species, will be needed to derive a general model that is applicable to other systems.

8 - References

1. Higman, C. and M. Van der Burgt, *Gasification*. 2011: Gulf professional publishing.
2. Milne, T.A., N. Abatzoglou, and R.J. Evans, *Biomass gasifier" tars": their nature, formation, and conversion*. 1998: National Renewable Energy Laboratory Golden, CO.
3. Rauch, R., et al., *Comparison of different olivines for biomass steam gasification*. 2004: na.
4. Grootjes, A., et al., *Improved Gasifier availability with bed material and additives.* 2013.
5. Berdugo Vilches, T., et al., *Comparing Active Bed Materials in a Dual Fluidized Bed Biomass Gasifier - Olivine, Bauxite, Sand and Ilmenite.* Submitted for publication, 2016.
6. Bergman, P.C., S.V. van Paasen, and H. Boerrigter. *The novel "OLGA" technology for complete tar removal from biomass producer gas*. in *Pyrolysis and Gasification of Biomass and Waste, Expert Meeting, Strasbourg, France*. 2002.
7. Dayton, D., *A review of the literature on catalytic biomass tar destruction.* NREL Report, NREL/TP-510-32815, NREL, Golden, CO, 2002.
8. Lind, F., M. Seemann, and H. Thunman, *Continuous catalytic tar reforming of biomass derived raw gas with simultaneous catalyst regeneration.* Industrial & Engineering Chemistry Research, 2011. **50**(20): p. 11553-11562.
9. Lyngfelt, A., B. Leckner, and T. Mattisson, *A fluidized-bed combustion process with inherent CO_2 separation; application of chemical-looping combustion.* Chemical Engineering Science, 2001. **56**(10): p. 3101-3113.
10. Thunman, H., et al., *Using an oxygen-carrier as bed material for combustion of biomass in a 12-MW th circulating fluidized-bed boiler.* Fuel, 2013. **113**: p. 300-309.
11. Thunman, H., N. Berguerand, and M. Seemann. *Advanced Gas Cleaning using Chemical-Looping Reforming (CLR)*. in *1st International Conference on Renewable Energy Gas Technology, Malmö 2014*. 2014.
12. Ahmadi, M., et al., *Development of an on-line tar measurement method based on photo ionization technique.* Catalysis Today, 2011. **176**(1): p. 250-252.
13. Meng, X., et al., *Tar formation in a steam-O_2 blown CFB gasifier and a steam blown PBFB gasifier (BabyHPR): Comparison between different on-line measurement techniques and the off-line SPA sampling and analysis method.* Fuel Processing Technology, 2012. **100**: p. 16-29.
14. Mitsakis, P., et al., *Optical measurement of tars in a fluidized bed gasifier: influence of fuel type and gasification parameters on their formation.* Biomass Conversion and Biorefinery, 2013: p. 1-11.

15. Moersch, O., H. Spliethoff, and K. Hein, *Tar quantification with a new online analyzing method.* Biomass and Bioenergy, 2000. **18**(1): p. 79-86.
16. Patuzzi, F., et al., *A comparison between on-line and off-line tar analysis methods applied to common reed pyrolysis.* Fuel, 2013.
17. Neeft, J., et al., *Guideline for sampling and analysis of tars and particles in biomass producer gases.*
18. Brage, C., et al., *Use of amino phase adsorbent for biomass tar sampling and separation.* Fuel, 1997. **76**(2): p. 137-142.
19. Osipovs, S., *Comparison of efficiency of two methods for tar sampling in the syngas.* Fuel, 2013. **103**: p. 387-392.
20. Israelsson, M., M. Seemann, and H. Thunman, *Assessment of the Solid-Phase Adsorption method for sampling biomass-derived tar in industrial environments.* Energy & Fuels, 2013. **27**(12): p. 7569-7578.
21. Neves, D., et al., *Method for online measurement of the CHON composition of raw gas from biomass gasifier.* Applied Energy, 2014. **113**: p. 932-945.
22. Cypres, R., *Aromatic hydrocarbons formation during coal pyrolysis.* Fuel Processing Technology, 1987. **15**: p. 1-15.
23. Font Palma, C., *Model for biomass gasification including tar formation and evolution.* Energy & Fuels, 2013. **27**(5): p. 2693-2702.
24. Fuentes-Cano, D., et al., *Kinetic modeling of tar and light hydrocarbons during the thermal conversion of biomass.* Energy & Fuels, 2015.
25. Corella, J., et al., *Two advanced models for the kinetics of the variation of the tar composition in its catalytic elimination in biomass gasification.* Industrial & engineering chemistry research, 2003. **42**(13): p. 3001-3011.
26. Gerun, L., et al., *Numerical investigation of the partial oxidation in a two-stage downdraft gasifier.* Fuel, 2008. **87**(7): p. 1383-1393.
27. Nguyen, H.N.T., N. Berguerand, and H. Thunman, *Mechanism and Kinetics of Catalytic Upgrading of a Biomass-Derived Raw Gas: An Application With Ilmenite as Catalyst.* Submitted for publication, 2016.
28. Morf, P., P. Hasler, and T. Nussbaumer, *Mechanisms and kinetics of homogeneous secondary reactions of tar from continuous pyrolysis of wood chips.* Fuel, 2002. **81**(7): p. 843-853.
29. Su, Y., et al., *Experimental and numerical investigation of tar destruction under partial oxidation environment.* Fuel Processing Technology, 2011. **92**(8): p. 1513-1524.
30. Bruinsma, O.S., et al., *Gas phase pyrolysis of coal-related aromatic compounds in a coiled tube flow reactor: 1. Benzene and derivatives.* Fuel, 1988. **67**(3): p. 327-333.
31. Bruinsma, O.S., et al., *Gas phase pyrolysis of coal-related aromatic compounds in a coiled tube flow reactor: 2. Heterocyclic compounds, their benzo and dibenzo derivatives.* Fuel, 1988. **67**(3): p. 334-340.
32. Jess, A., *Mechanisms and kinetics of thermal reactions of aromatic hydrocarbons from pyrolysis of solid fuels.* Fuel, 1996. **75**(12): p. 1441-1448.
33. Evans, R.J. and T.A. Milne, *Molecular characterization of the pyrolysis of biomass.* Energy & Fuels, 1987. **1**(2): p. 123-137.
34. Evans, R.J. and T.A. Milne, *Molecular characterization of the pyrolysis of biomass. 2. Applications.* Energy & fuels, 1987. **1**(4): p. 311-319.
35. Kiel, J., et al., *Primary measures to reduce tar formation in fluidised-bed biomass gasifiers.* ECN, ECN-C-04-014, 2004.
36. Williams, P.T. and D.T. Taylor, *Aromatization of tyre pyrolysis oil to yield polycyclic aromatic hydrocarbons.* Fuel, 1993. **72**(11): p. 1469-1474.

37. Fuentes-Cano, D., et al., *The influence of temperature and steam on the yields of tar and light hydrocarbon compounds during devolatilization of dried sewage sludge in a fluidized bed.* Fuel, 2013. **108**: p. 341-350.
38. Fitzpatrick, E., et al., *Mechanistic aspects of soot formation from the combustion of pine wood.* Energy & Fuels, 2008. **22**(6): p. 3771-3778.
39. Dufour, A., et al., *Evolution of aromatic tar composition in relation to methane and ethylene from biomass pyrolysis-gasification.* Energy & Fuels, 2011. **25**(9): p. 4182-4189.
40. Scott, D. and J. Piskorz, *The flash pyrolysis of aspen-poplar wood.* The Canadian Journal of Chemical Engineering, 1982. **60**(5): p. 666-674.
41. Min, Z., et al., *Catalytic reforming of tar during gasification. Part I. Steam reforming of biomass tar using ilmenite as a catalyst.* Fuel, 2011. **90**(5): p. 1847-1854.
42. Devi, L., K.J. Ptasinski, and F.J. Janssen, *A review of the primary measures for tar elimination in biomass gasification processes.* Biomass and Bioenergy, 2003. **24**(2): p. 125-140.
43. Larsson, A., *FUEL CONVERSION IN A DUAL FLUIDIZED BED GASIFIER*. 2014: Chalmers University of Technology.
44. Neves, D.d.S.F.d., *Evaluation of thermochemical biomass conversion in fluidized bed.* 2013.
45. Larsson, A., et al., *Evaluation of Performance of Industrial-Scale Dual Fluidized Bed Gasifiers Using the Chalmers 2–4-MWth Gasifier.* Energy & Fuels, 2013.
46. Kaufman Rechulski, M., et al., *Liquid-Quench Sampling System for the Analysis of Gas Streams from Biomass Gasification Processes. Part 2: Sampling Condensable Compounds.* Energy & Fuels, 2012. **26**(10): p. 6358-6365.
47. Osipovs, S., *Sampling of benzene in tar matrices from biomass gasification using two different solid-phase sorbents.* Analytical and Bioanalytical Chemistry, 2008. **391**(4): p. 1409-1417.
48. Van Paasen, S. and J. Kiel, *Tar formation in fluidised-bed gasification-impact of gasifier operating conditions.* Acknowledgement/Preface, 2004: p. 26.
49. Kinoshita, C., Y. Wang, and J. Zhou, *Tar formation under different biomass gasification conditions.* Journal of Analytical and Applied Pyrolysis, 1994. **29**(2): p. 169-181.
50. Hofbauer, H. and R. Rauch, *Stoichiometric water consumption of steam gasification by the FICFB-gasification process.* Progress in thermochemical biomass conversion, 2000. **1**: p. 199-208.
51. Kitzler, H., C. Pfeifer, and H. Hofbauer, *Pressurized gasification of woody biomass—variation of parameter.* Fuel Processing Technology, 2011. **92**(5): p. 908-914.
52. Pfeifer, C., R. Rauch, and H. Hofbauer, *In-bed catalytic tar reduction in a dual fluidized bed biomass steam gasifier.* Industrial & engineering chemistry research, 2004. **43**(7): p. 1634-1640.
53. Abdelouahed, L., et al., *Detailed modeling of biomass gasification in dual fluidized bed reactors under Aspen Plus.* Energy & Fuels, 2012. **26**(6): p. 3840-3855.
54. Elliott, D.C. and E.G. Baker, *The effect of catalysis on wood-gasification tar composition.* Biomass, 1986. **9**(3): p. 195-203.
55. Sutton, D., B. Kelleher, and J.R. Ross, *Review of literature on catalysts for biomass gasification.* Fuel Processing Technology, 2001. **73**(3): p. 155-173.
56. Marinkovic, J., et al., *Characteristics of olivine as a bed material in an indirect biomass gasifier.* Chemical Engineering Journal, 2015. **279**: p. 555-566.

57. Davidsson, K.O., et al., *A surface ionization instrument for on-line measurements of alkali metal components in combustion: Instrument description and applications.* Energy & fuels, 2002. **16**(6): p. 1369-1377.
58. Sette, E., D. Pallarès, and F. Johnsson, *Experimental quantification of lateral mixing of fuels in fluid-dynamically down-scaled bubbling fluidized beds.* Applied Energy, 2014. **136**: p. 671-681.
59. Yang, Y., J. Mulholland, and U. Akki. *Formation of furans by gas-phase reactions of chlorophenols*. in *Symposium (International) on Combustion*. 1998. Elsevier.

Paper I

Paper II

Paper III

Paper IV

Paper V

Paper VI